Rare Earth-Transition Metal Compounds: Magnetism and Applications

E.Burzo

Faculty of Physics, Babes-Bolyai University, Cluj-Napoca, Romania

1. Phase Diagrams
2. Magnetic Properties
   - Exchange enhanced paramagnets
   - Induced transition moments, at H_{cr}
   - Exchange interactions

3. Technical applications

3.1 Permanent magnets

$SmCo_5$

$Sm(Co,Fe,Zr,Cu)_z$

Nd-Fe-B

Nanocrystalline magnets

3.2 Magnetostrictive materials RFe_2

3.3 Magnetocaloric materials

3.4 Hydrogen storage

1. Phase diagrams R-M, R = rare-earth, M = Mn,Fe,Co,Ni

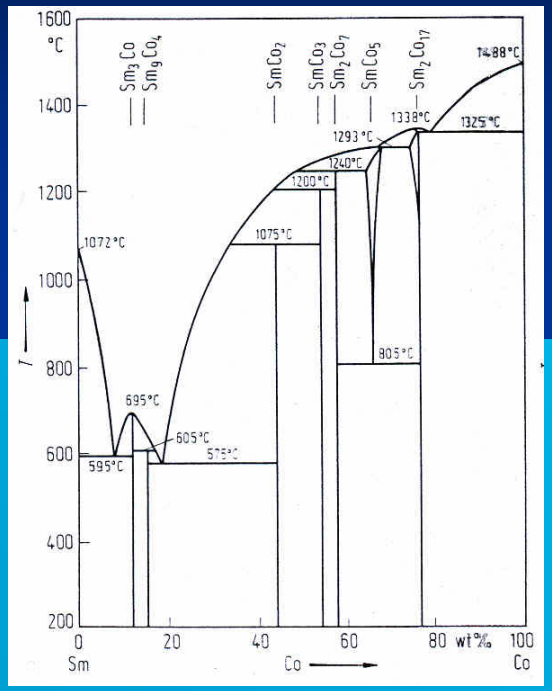

Fig.1

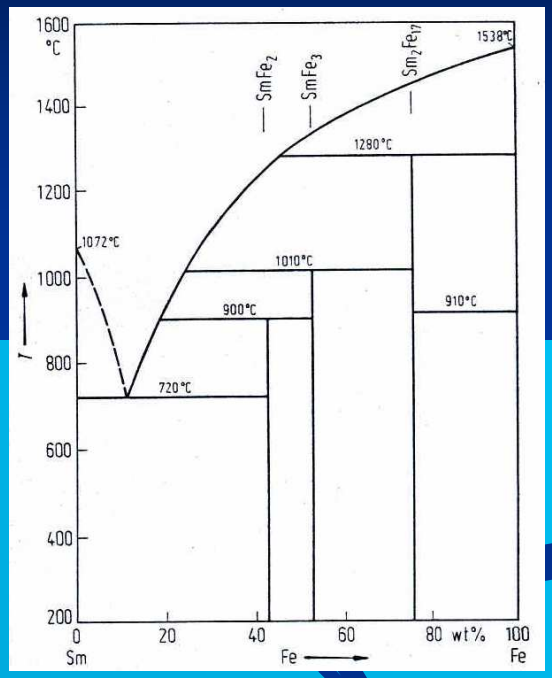

Fig.2

$r_R/r_M \cong 1.4$

- Formed by peritectic reaction
- At least one eutetic
- Number of compounds increase from M= Mn to M= Ni

Crystal structures

$MgCu_2$	C15	RM_2
$CaCu_5$	hex	RM_5

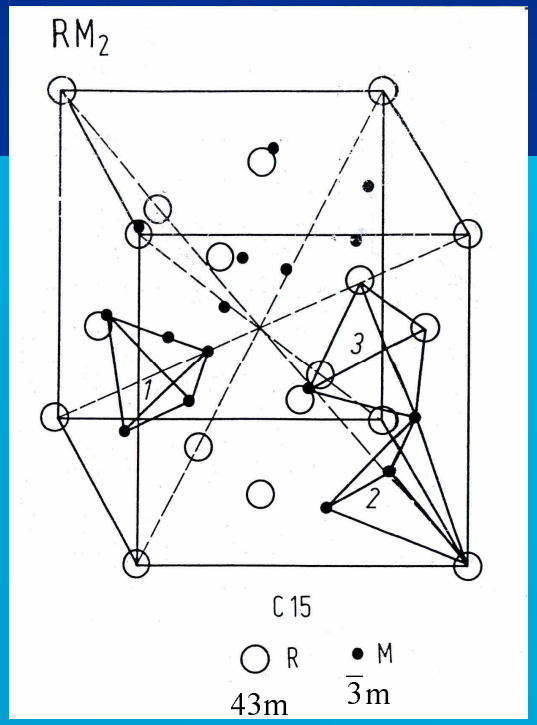

Fig.3

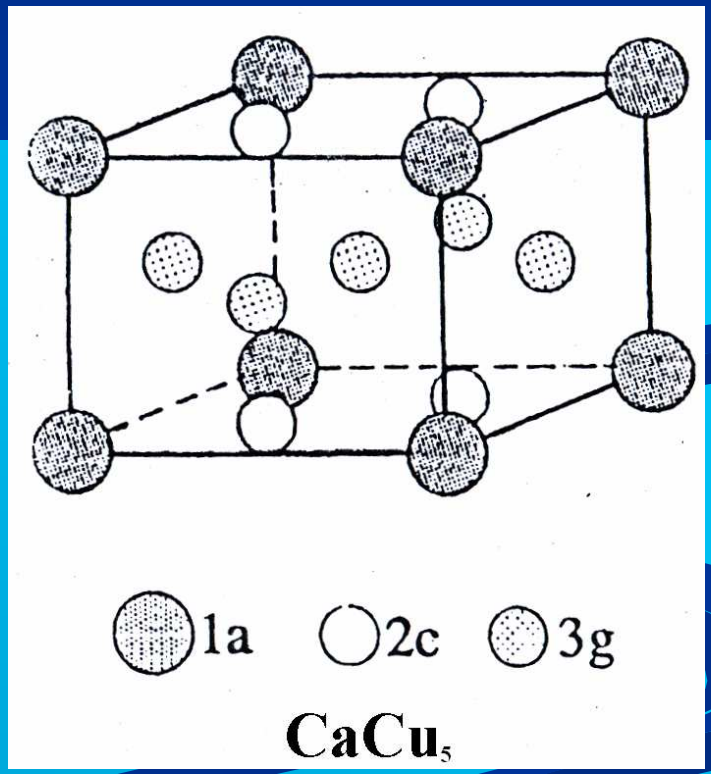

Fig.4

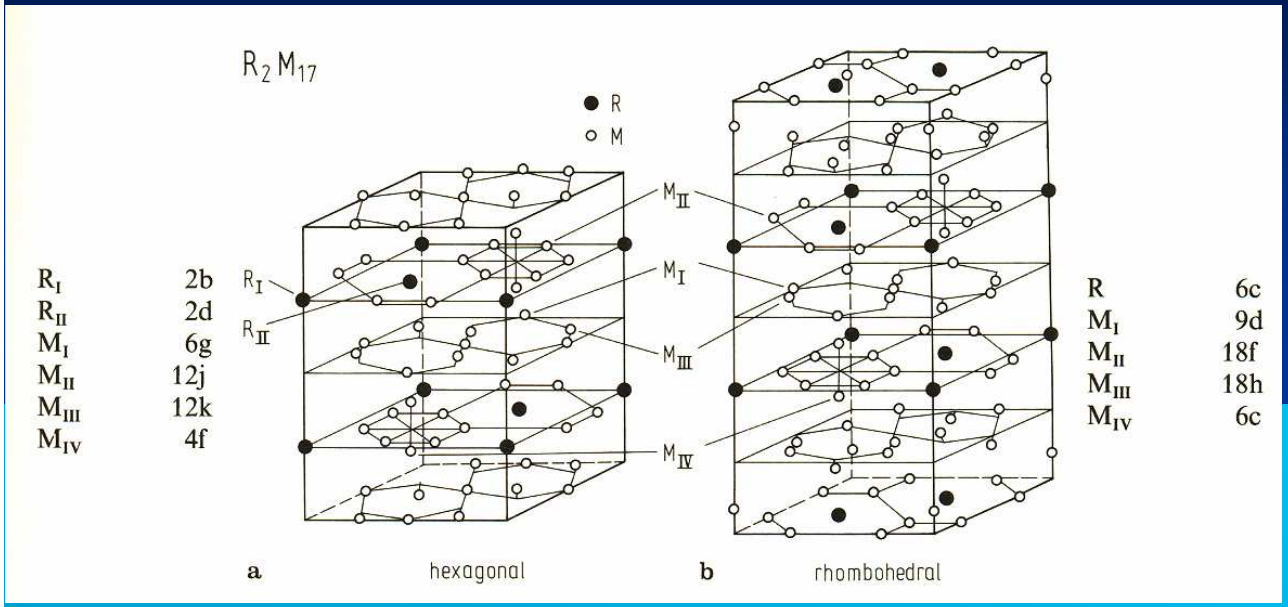

Fig.5

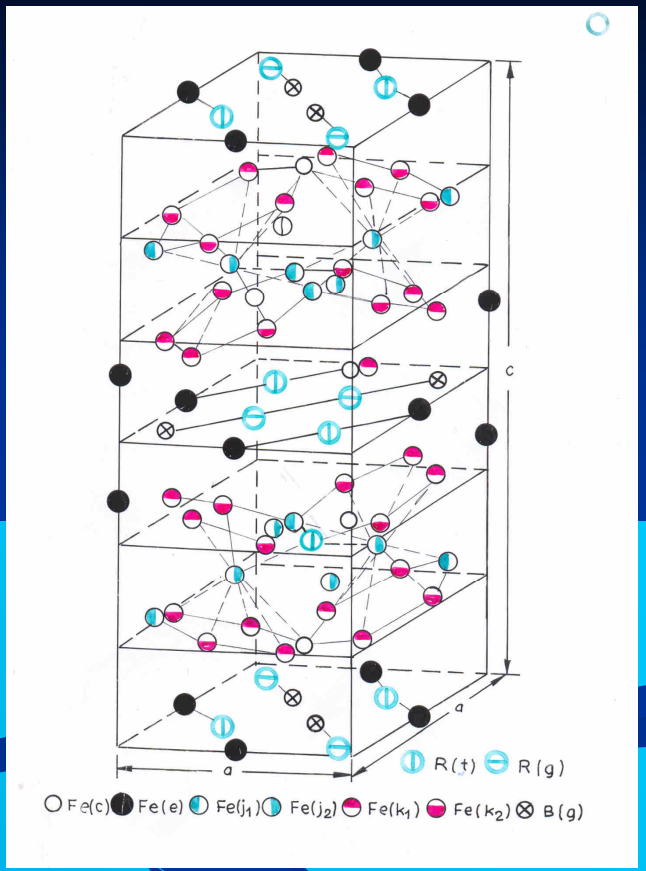

Fig.6

Hexagonal (Th_2Ni_{17}-type) R_2M_{17} $P6_3/mmc$

Rhombohedral(Th_2Zn_{17}-type) R_2M_{17} $R\bar{3}m$

2. Magnetic properties R-M compounds

R: 4f electrons, small spatial extent (well localized)

La,Lu, (Y) nonmagnetic

M:3d electrons

onset

well established magnetism

collapse

exchange enhanced paramagnetism

Magnetism of transition metals in rare-earth compounds

2.1 Magnetic propertis of exchange enhanced paramagnet

2.2 Induced transition metal moment, H_{cr}

2.3 Magnetic behaviour of Co,Ni,Fe at $H > H_{cr}$.

Magnetic coupling

M_R ↑ ↑ M_M

R-light rare-earth

M_R ↑ ↓ M_M

R-heavy rare earth

4f-5d-3d type

2.1 Exchange enhanced paramagnet

Co exchange enhanced paramagnets

YCo_2 $LuCo_2$

$Y(Co_{1-x}Ni_x)_2$

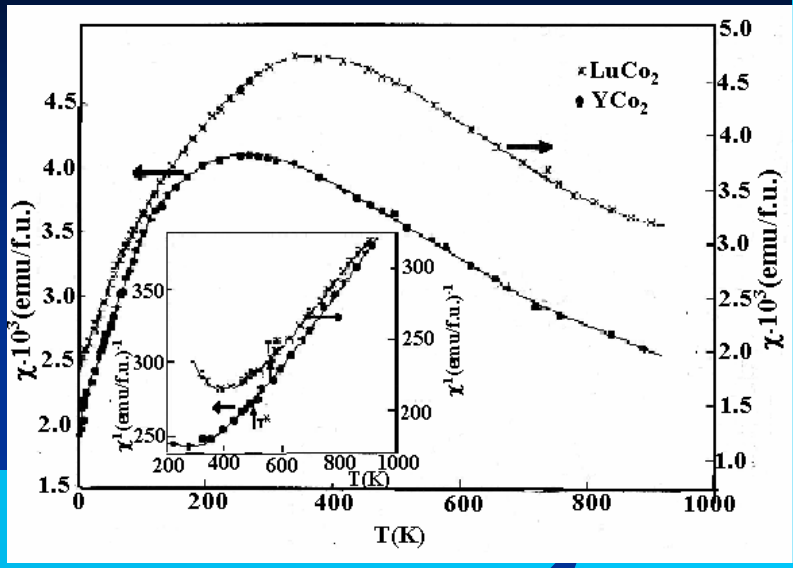

Fig.7

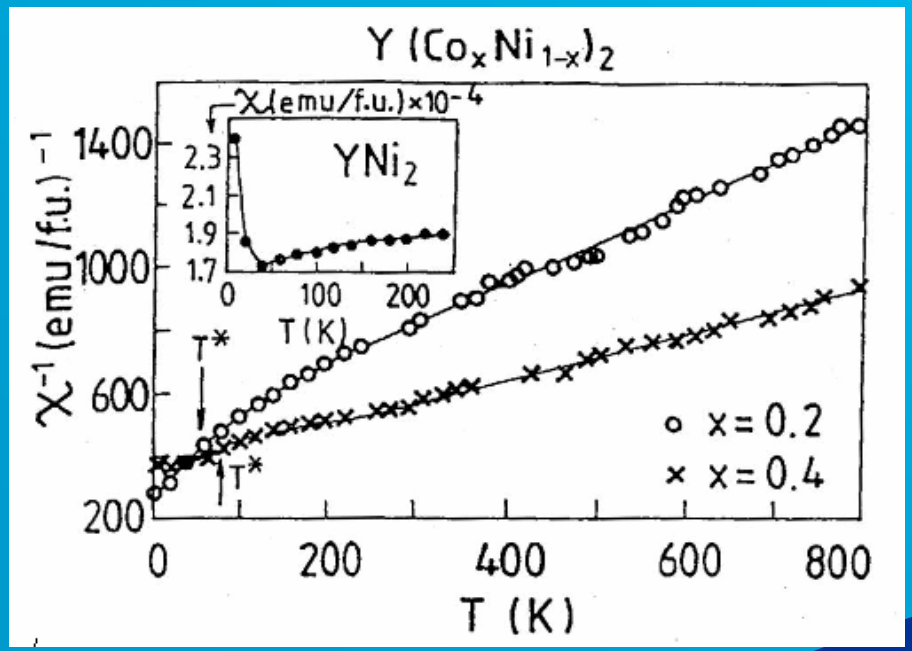

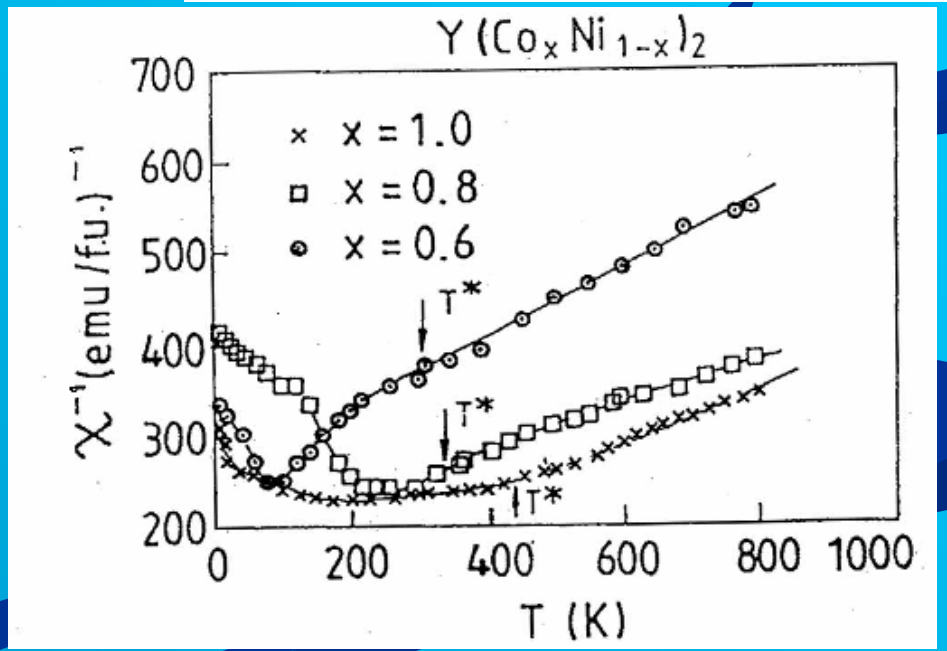

Fig.8

$T \leq 10\ K \qquad \chi = \chi_o(1+aT^2)$

$T > T^*$ Curie Weiss – type behaviour $\chi = C(T-\theta)^{-1}$; $\theta<0$

$Y(Co_{1-x}Ni_x)_2$ $M_{eff}(Co)$ little dependent on composition

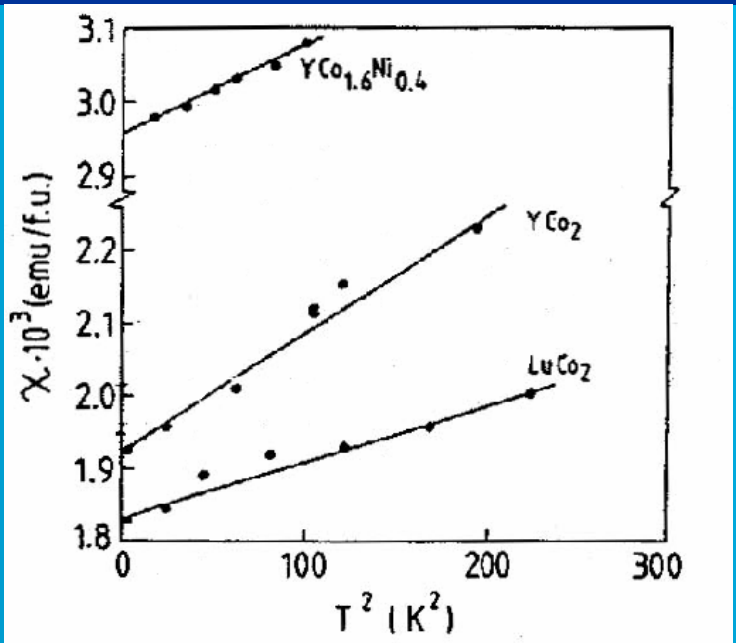

Fig.9

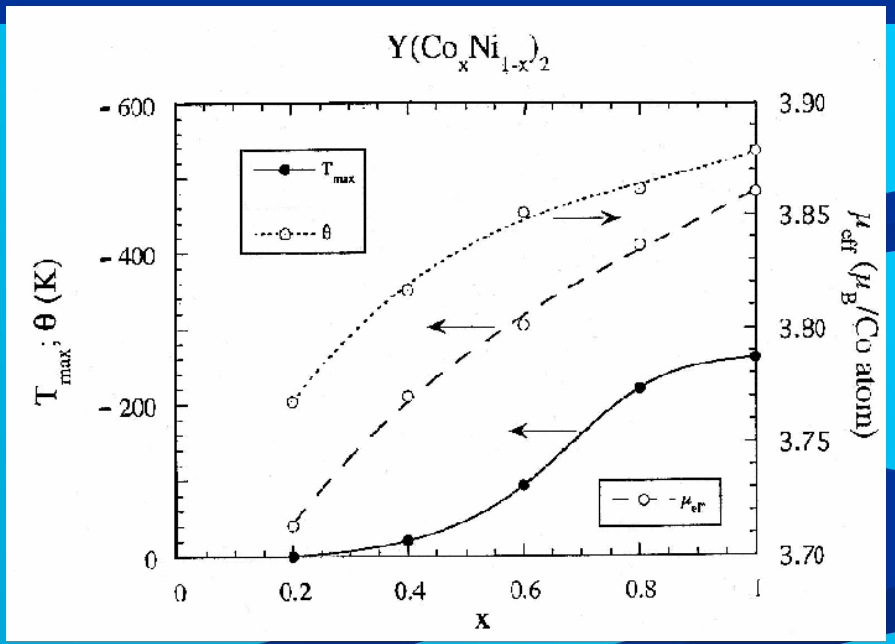

Fig.10

$Y(Co_{1-x}Si_x)_2$ high decrease of $M_{eff}(Co)$

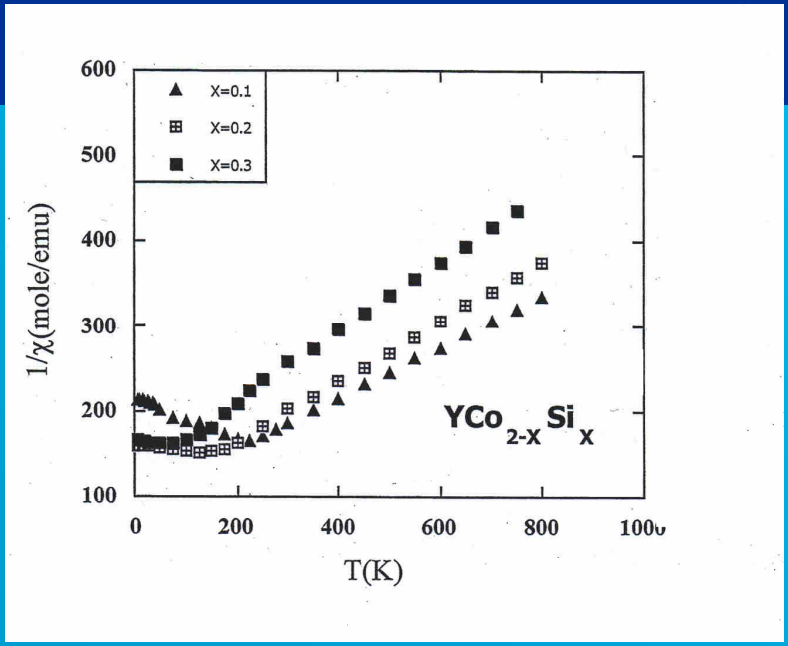

Fig.11

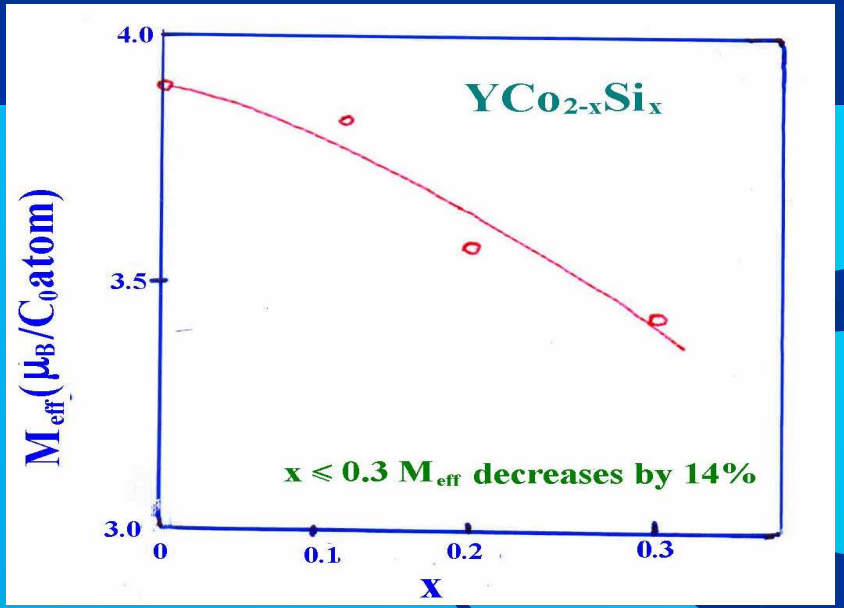

Fig.12

$YCo_{3-x}Ni_xB_2$

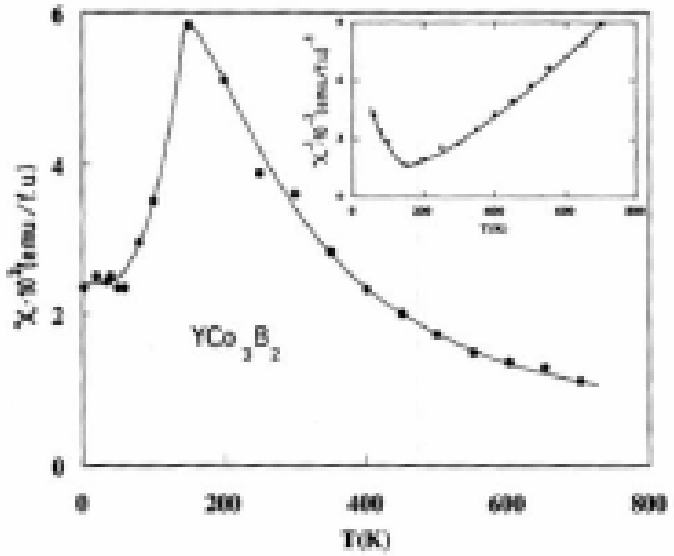

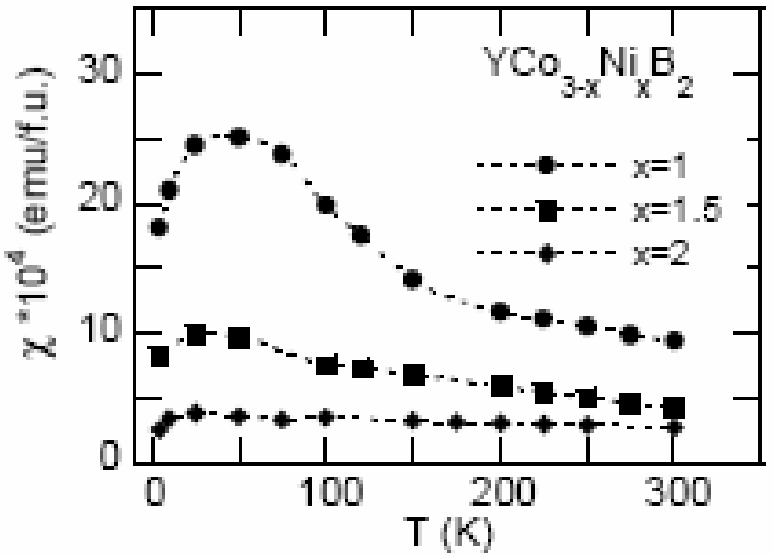

Fig.13

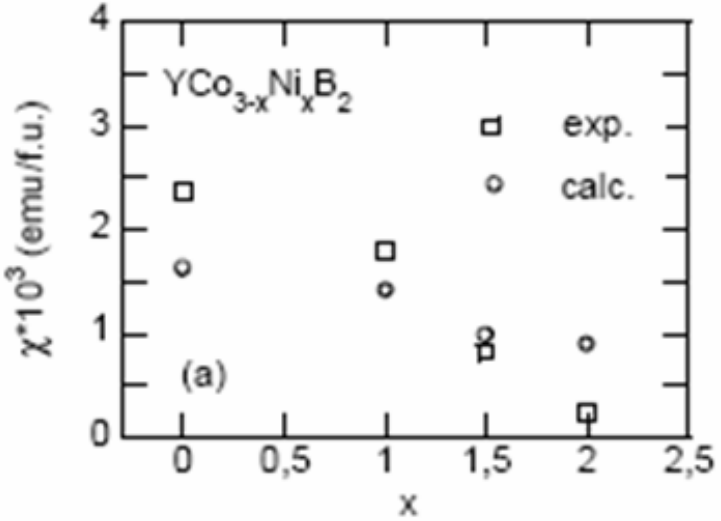

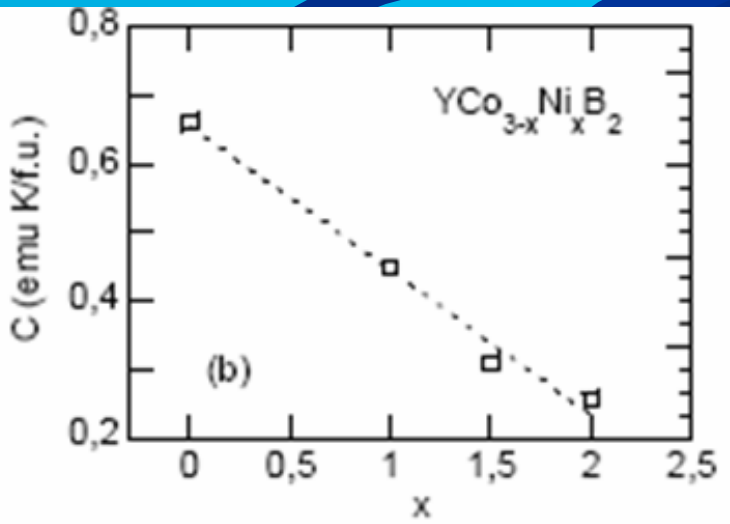

Fig.14

Band structure calculations: LMTO-ASA

$Y(Co_{1-x}Ni_x)_2$

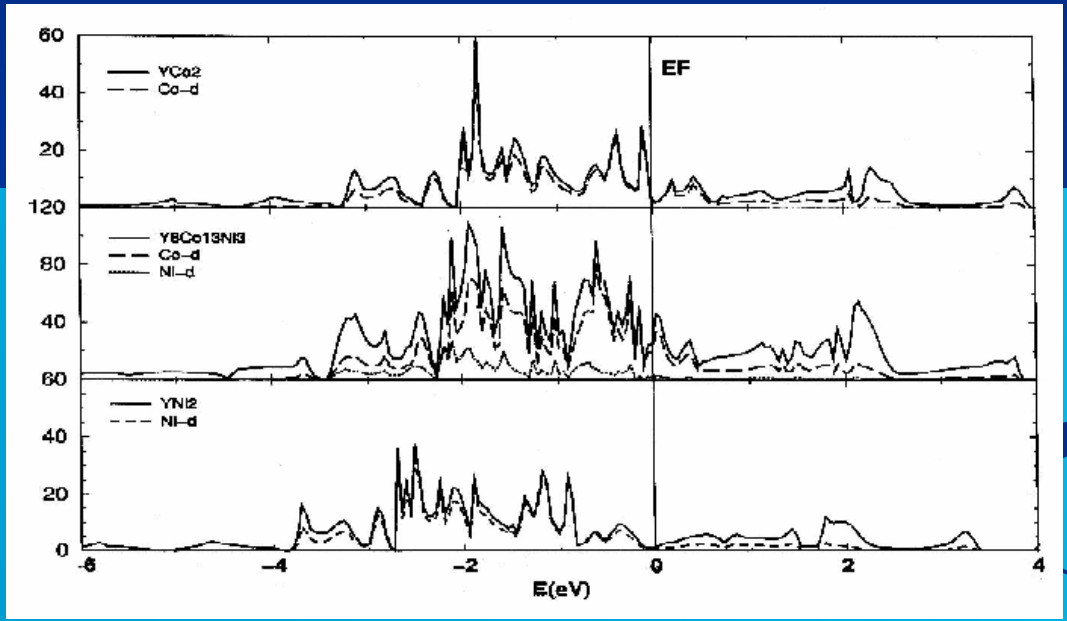

Fig.15

$Y(Co_{1-x}Si_x)_2$ Hybridization effect Co 3d-Si2p bands

↓

double peak is broadened by p-d hybridization

Co3d band shifted to lower energy

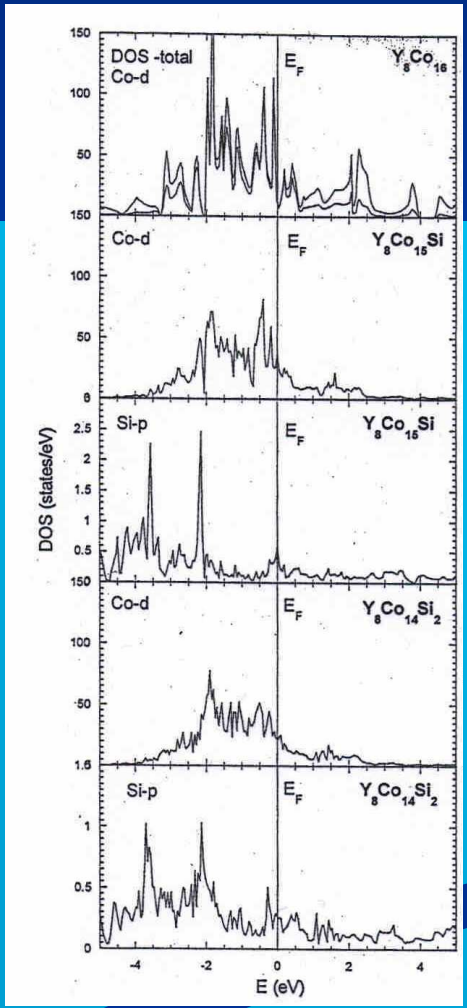

Fig.16

Compound	χ_{exp} at 1.7 K (emu/fu)·10^3	χ_{calc} (emu/fu)·10^3	a_{exp} (K^{-2})·10^{-6}	a_{calc} (K^{-2})·10^{-6}
YCo_2	1.90	1.80	1.2	1.1
$YCo_{1.6}Ni_{0.4}$	2.50	2.80	1.30	1.5

$$\chi = \chi_o(1+aT^2)$$

Self consistent theory of spin fluctuations

Wave number dependent susceptibility, χ_q, for a nearly ferromagnetic alloy has a large enhancement for small q values

$$\chi_q = \frac{\overline{\chi}_q}{1 - J\overline{\chi}_q(\mu_0\mu_B^2)}$$

Frequency of longitudinal spin fluctuations $\omega^* \propto \frac{1}{\tau}$

τ-lifetime of LSF

Low temperature

$$\omega^* < \frac{k_B T}{\hbar}$$ (thermal fluctuations-transversal slow)

$$\chi = s\chi_p\left[1 + \frac{\pi^2}{6}\left(2\frac{\eta''}{\eta} - 1.2\frac{\eta'^2}{\eta^2}\right)_{E_F} s^2T^2\right]$$

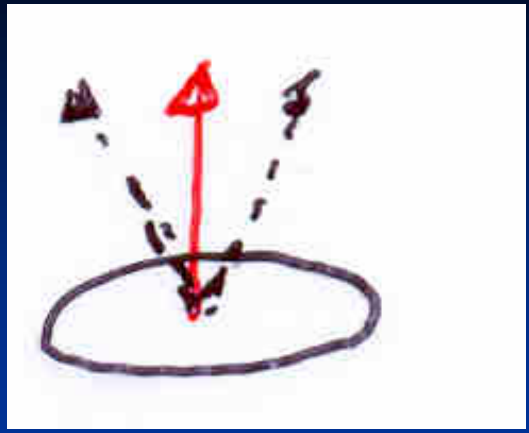

Approximation for nonmagnetic state

$$\chi \propto T^2$$

$\chi(T)$ ↗ as T ↗

$\eta'' > 0$ (necessary condition, not sufficient)

High temperature

Average mean amplitude of LSF is temperature dependent

$$\left\langle S_{loc}^2 \right\rangle = 3k_B T \sum_q \chi_q$$

S_{loc} ↗ as T ↗ up to T* (S_{loc})

S_{loc} determined by charge neutrality condition

The system behaves as having local moments for temperatures T > T* where the frequency of spin fluctuations

$$\omega^* < \frac{k_B T}{\hbar}$$

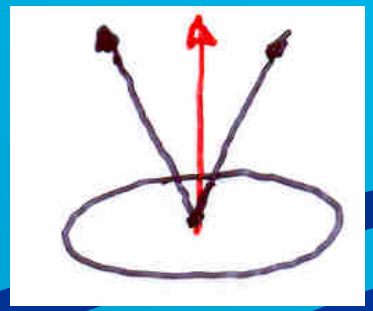

S_{loc}

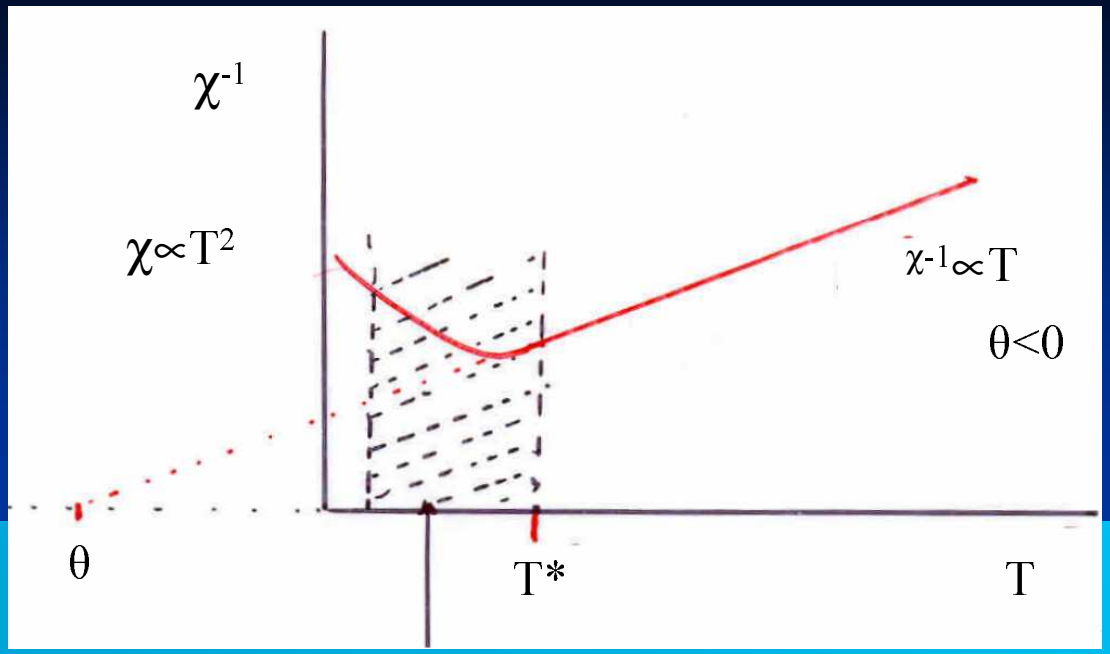

C-W type

Crossover between low T regime governed by spin fluctuations and high T classical regime

Gaussian distribution of spin fluctuations (Yamada)

$$\chi_s^{-1} = a_1 - \alpha + \frac{5}{3}a_3 s^2 + \frac{35}{9}a_5 s^4 + \frac{35}{3}a_7 s^6 + \ldots \qquad (2)$$

where the mean square value of the fluctuating magnetization, s^2, is given by:

$$\langle s^2 \rangle = \frac{3}{2\pi^2} k_B T q_m A^{-1} \left(1 - \frac{tg^{-1}\left(q_m \sqrt{A\chi}\right)}{q_m \sqrt{A\chi}} \right) \qquad (3)$$

We denoted by a_1, a_3, a_5 and a_7 the expansion coefficients of the free energy with respect to the square of the magnetization density and α, q_m and A denote the molecular field coefficient, the cut-off wave vector of spin fluctuations and the exchange stiffness constant, respectively.

In the following we limit the series expansion development up to terms in s^2. The explicit expressions for a_i coefficients were given as:

$$a_1 = \frac{2}{g^2 \mu_B^2 N} \left\{ 1 + \frac{1}{6}(\pi k_B T)^2 \left[\left(\frac{N'}{N} \right)^2 - \frac{N''}{N} \right] + \ldots \right. \qquad (4)$$

$$a_3 = \frac{g^2 \mu_B^2}{2^2 3!} a_1^3 \left\{ 3\left(\frac{N'}{N} \right)^2 - \frac{N''}{N} + \frac{1}{6}(\pi k_B T)^2 \right.$$
$$\left. \left[6\left(\frac{N'}{N} \right)^4 - 13\frac{N'' N'^2}{N^3} + \left(\frac{N''}{N} \right)^2 + 7\left(\frac{N''' N'}{N^2} \right) - \frac{N''''}{N} \right] + \ldots \right\} \qquad (5)$$

We denoted by N the state density at the Fermi level and N', N'', N''' and N'''' are their derivatives of order to one up to four.

Composition	a (Å)	λ.	$q_m = \pi/a\lambda$. ($Å^{-1}$)	A ($cm^5 Oe^2/erg) 10^{-12}$
1.0	7.206	2.02	0.215	5.5
0.8	7.200	1.93	0.225	5.4
0.6	7.196	1.85	0.235	5.3
0.4	7.190	1.29	0.338	5.2
0.2	7.183	1.30	0.336	5.1

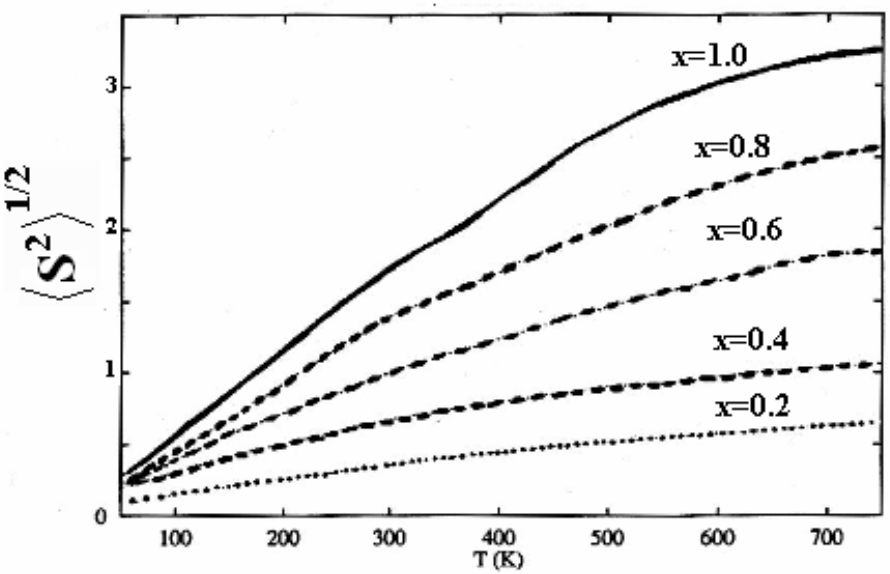

$Y(Co_xNi_{1-x})_2$

Fig.19

$Y(Co_xNi_{1-x})_2$

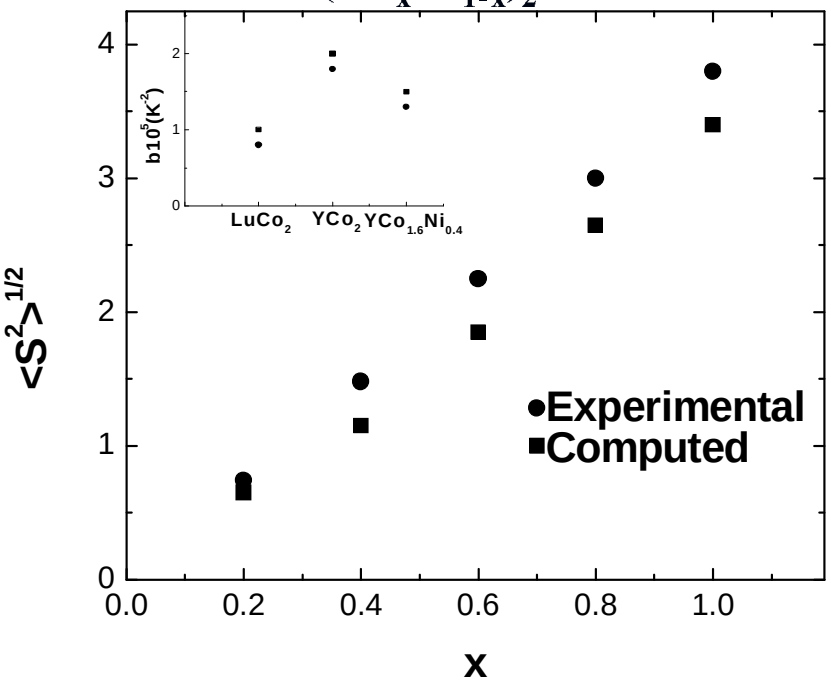

Fig.20

Quenching of spin fluctuations

•external field: Beal-Monod, Brinkman-Engelsberg

(theor. 1968)

Ikeda et al: specific heat

(exp. 1984)

•internal field: Burzo-Lemaire

(exp.1992)

If the magnetic field is sufficiently large so that the Zeeman splitting energy of opposite spin states is comparable to, or larger than the characteristic spin fluctuation energy ⇒ paramagnons no longer have sufficient energy to flip spins and the inelastic spin flip scattering is quenched.

$H_{quench} \propto T_{sf}$

Specific heat (10T) external field (Ikeda et al)

γ reduced by 4 % YCo_2

10 % $LuCo_2$

Magnetic measurements

RCo_2(R magnetic) M_{eff} ↘T_c ↗

$$M_{eff} = a + bH_{exch}^{-1} \qquad b = 1.7 \cdot 10^{-2}\ \mu_B T$$

For $\Delta H_{exch} = 10$ T ⇒ ΔM_{eff} decrease by 6 %

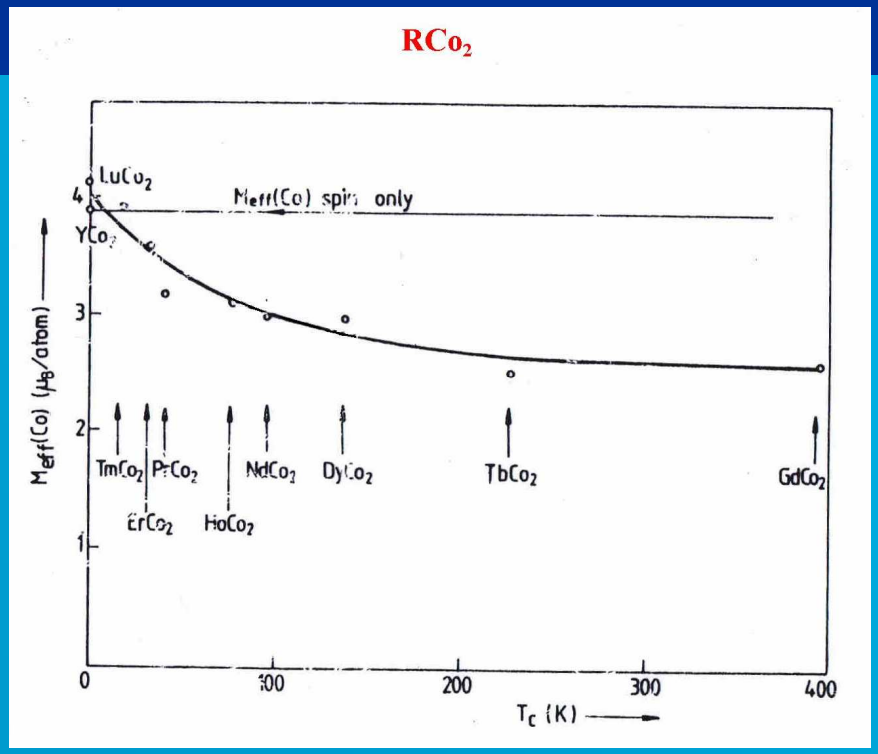

Fig.20

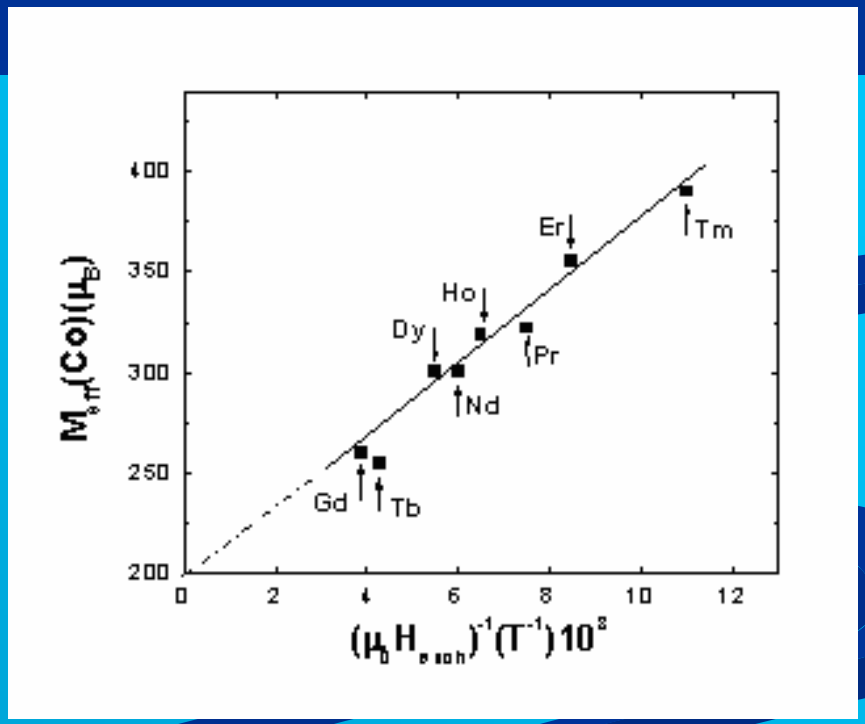

Fig.21

$LaNi_{5-x}Cu_x$; $LaNi_{5-x}Al_x$

Cu	$CaCu_5$ – type	$x \leq 2$
Al	$CaCu_5$ – type	$x < 2$
	$HoNi_{2.6}Ga_{2.4}$ – type	$x \geq 2$

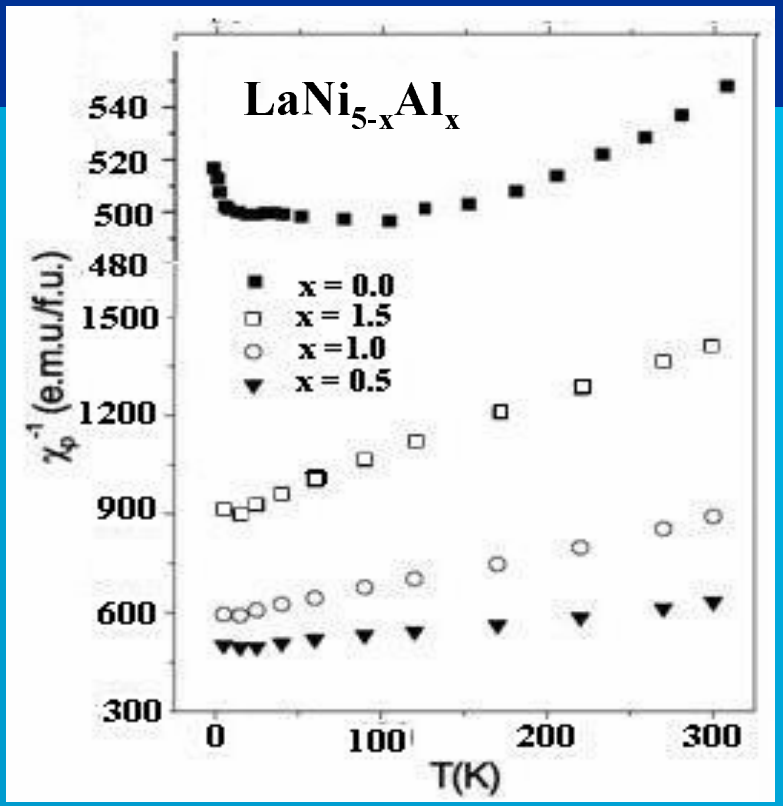

Fig.22

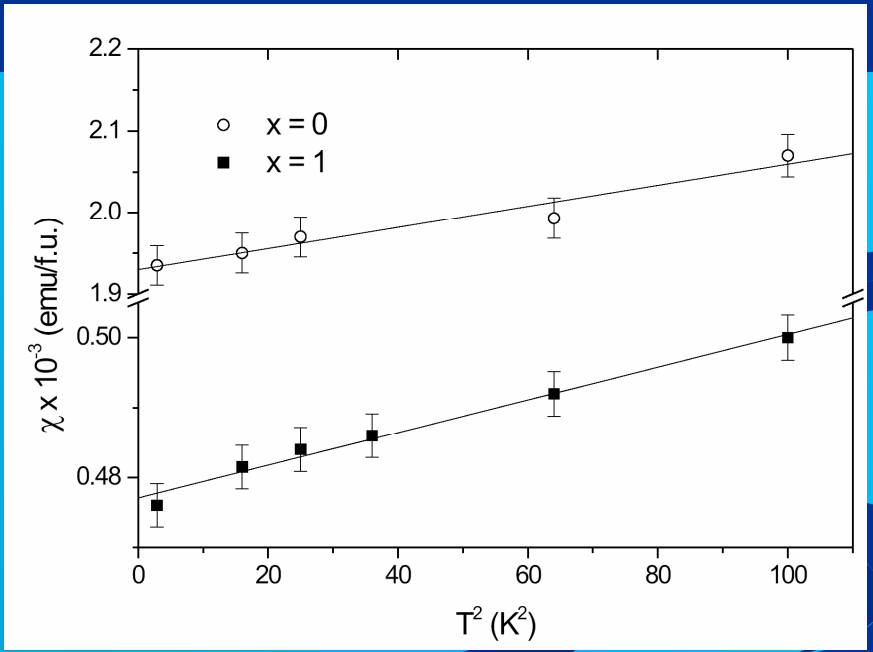

Fig.23

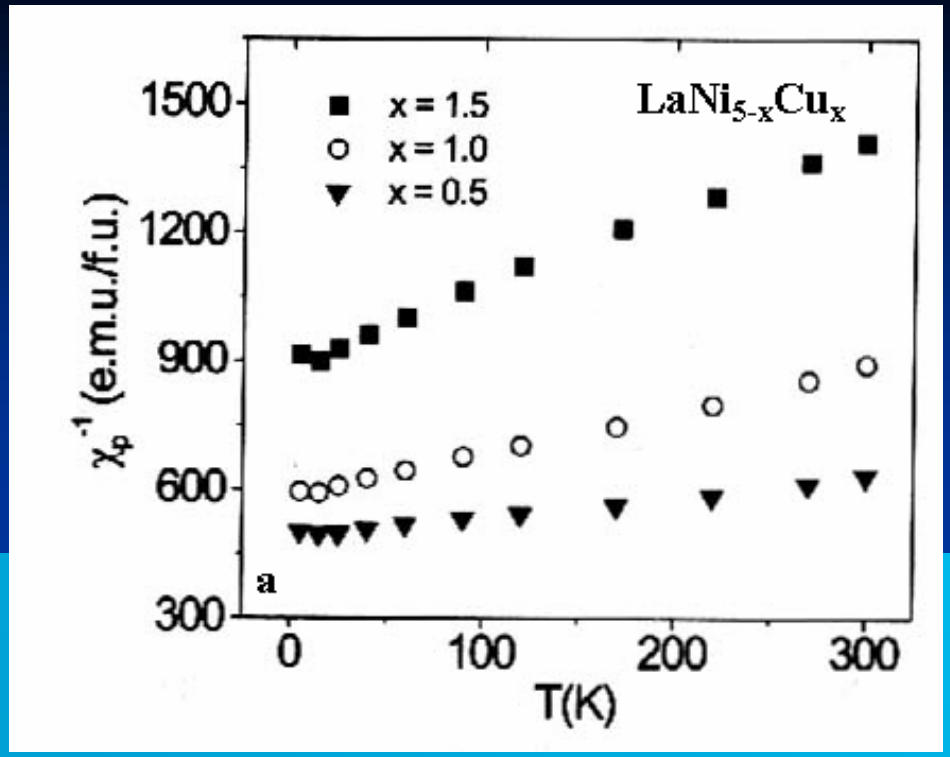
1500
1200
900
600
300
0
100
200
300
T(K)
χ_p^{-1} (e.m.u./f.u.)
x = 1.5
x = 1.0
x = 0.5
$LaNi_{5-x}Cu_x$
a

Fig.24

Fig.25

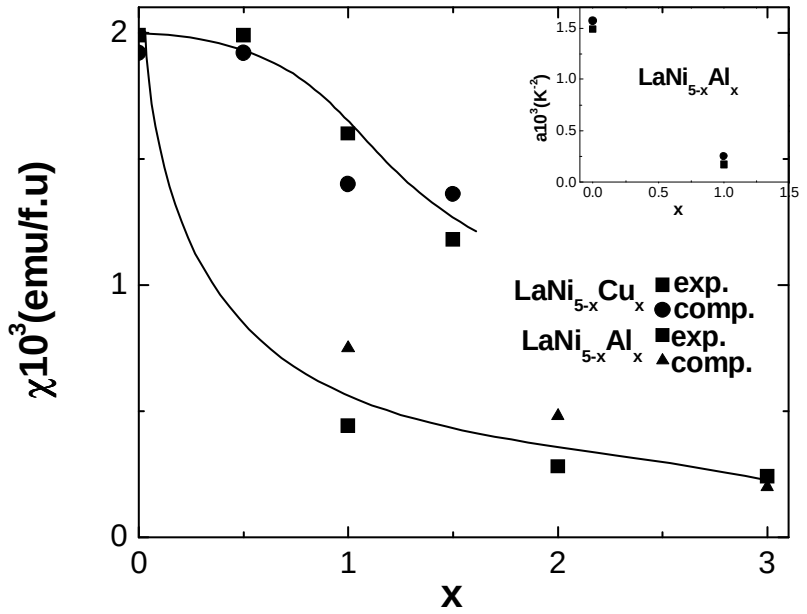
2
1
0
0
1
2
3
x
$\chi 10^3$(emu/f.u)
$LaNi_{5-x}Cu_x$ exp.
comp.
$LaNi_{5-x}Al_x$ exp.
comp.
$LaNi_{5-x}Al_x$
$a10^3(K^{-2})$
1.5
1.0
0.5
0.0
0.0
0.5
1.0
1.5
x

RT

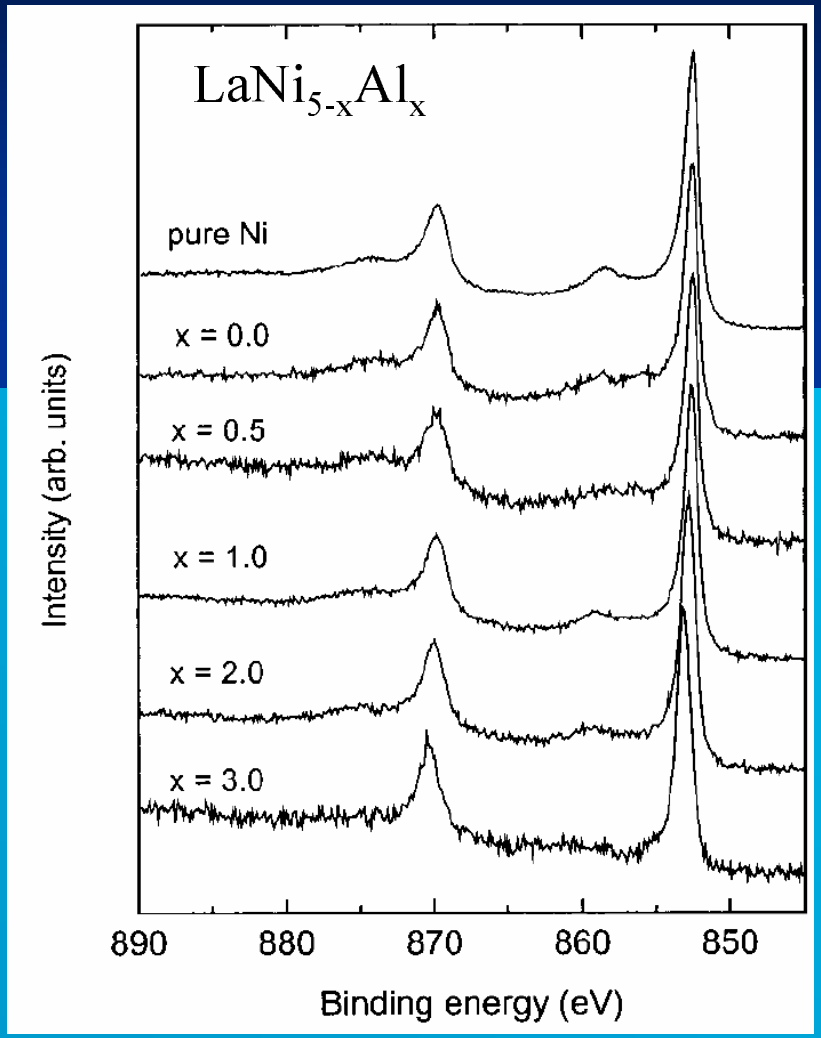

Fig.26

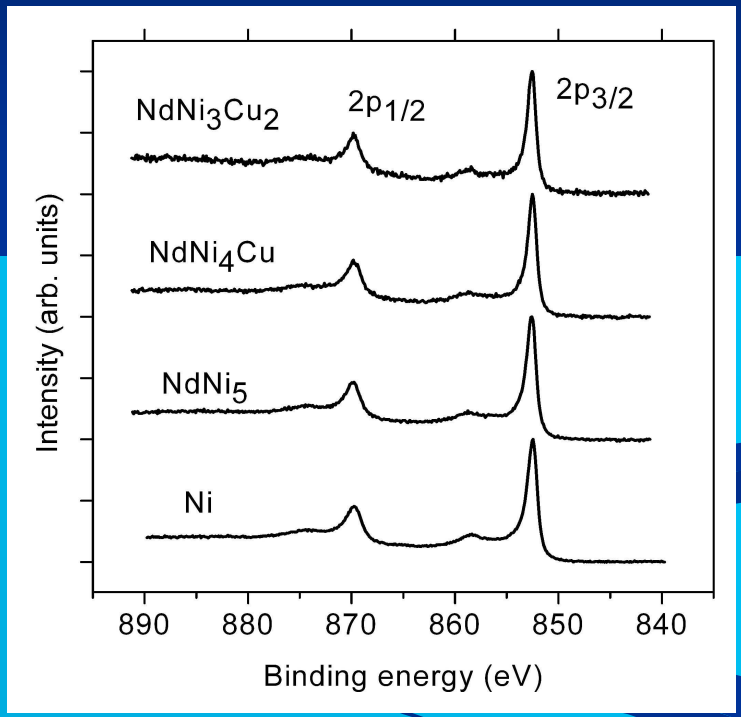

Fig.27

2.2 Induced transition metal moment

$(Gd_xY_{1-x})Co_2$ Lemaire, 1966

Critical field for appearance a magnetic moments

⇓

critical value of exchange interactions

$Gd(Co_xNi_{1-x})_2$ 1974

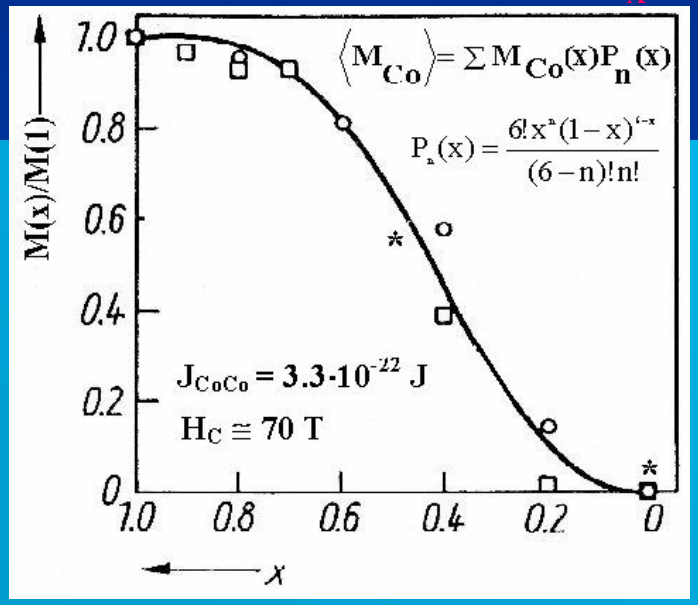

Fig.28

$\underline{n} \geq 3$ NN

$\bar{3}m$ site

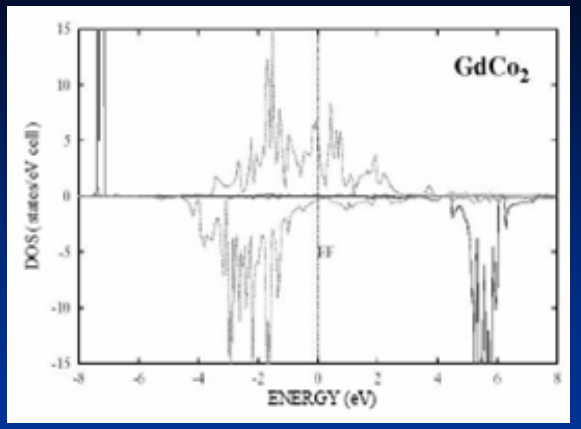

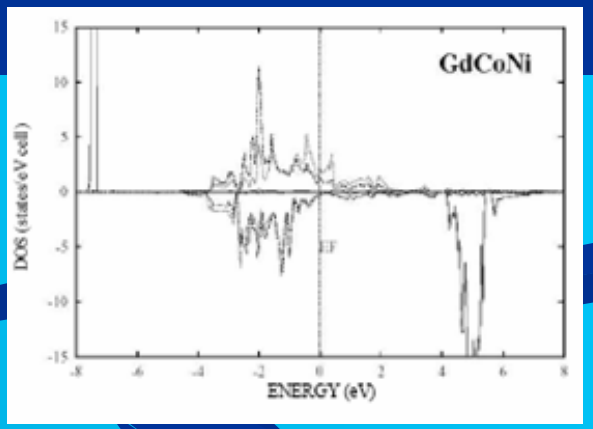

Fig.29

Band structures

$GdCo_2$ $M_{Co} = 1.20\ \mu_B$ $GdNi_2$ $M_{Ni} = 0.12\ \mu_B$

GdCoNi $M_{Co} = 1.12\ \mu_B$ $M_{Ni} = 0.17\ \mu_B$

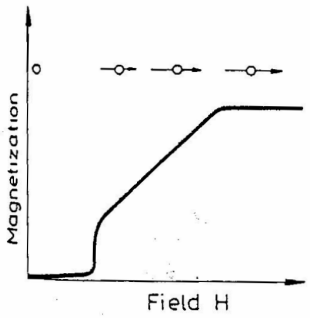

E.Burzo J.Less Common Met (1978)

The magnetization curve for induced magnet

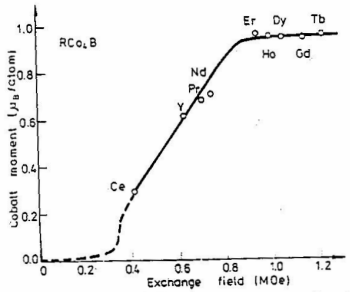

E.Burzo J.Less Common Met (1989)

Variation of the cobalt moment as function of the exchange field at 4.2 K in RCo_4B compounds.

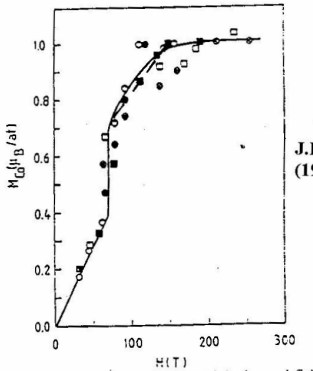

J.Franse J.Magn. Magn. Mat. (1992)

The Co-moment as a function of the internal field in $(R, Y)Co_2$: R = Gd ⊗, Tb □, Dy ■, Ho ○ and Er ●. Data from [3].

Fig.30

Field dependence of transition metal moment

$\Delta M_{Co} = V_{Co}\Delta H_{exch}$ $V_{Co} = (3\cdot10^6)^{-1}\mu_B/Oe$

High field measurements, Amsterdam: confirmed V_{Co} value

$\Delta M_{Fe} = V_{Fe}\Delta H_{exch}$ $V_{Fe} =(18\cdot10^6)^{-1}\ \mu_B/Oe$

Confirmed by high field measurements (Amsterdam) – cobalt compounds

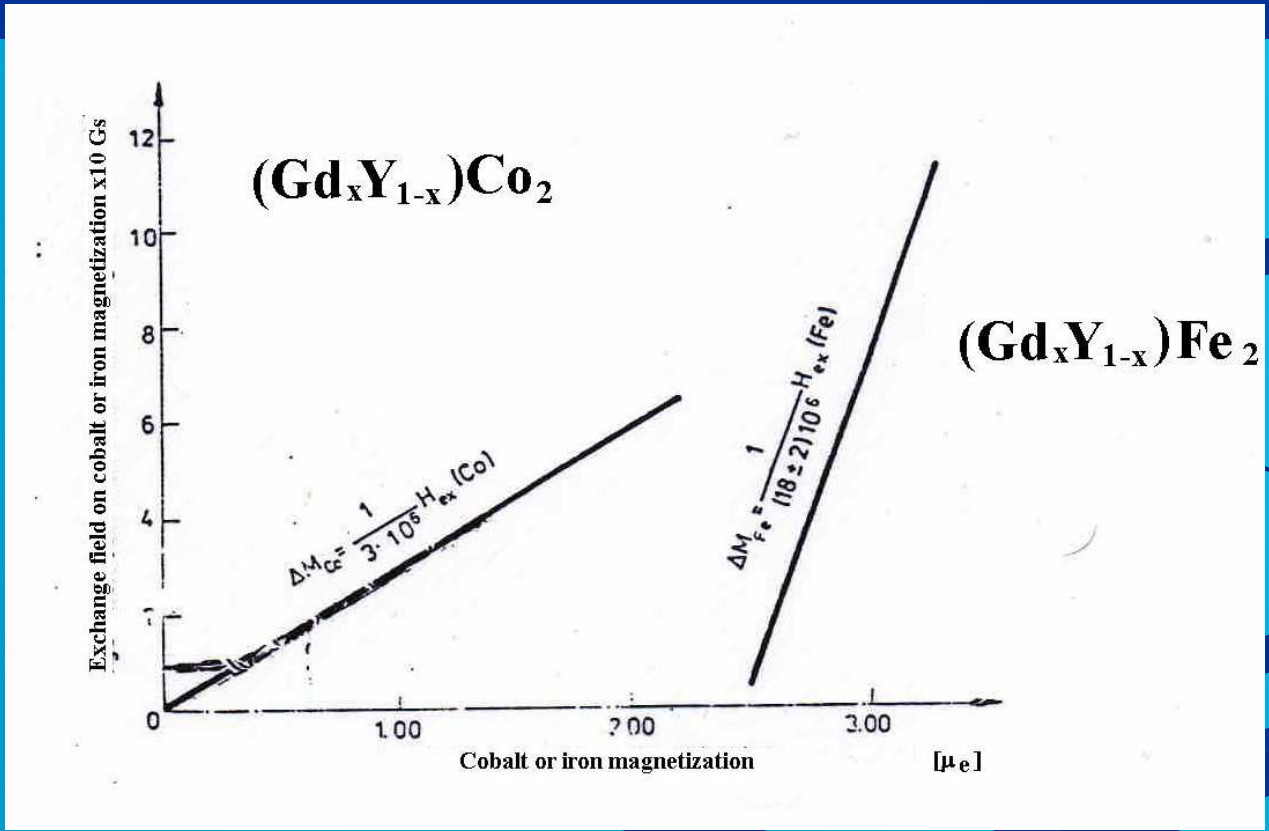

Fig.31

$Gd_xLa_{1-x}Ni_5$

0 K

$M_{Ni} \cong 0.20\ \mu_B$

$Ni \cong 0$

$GdNi_5$

$LaNi_5$

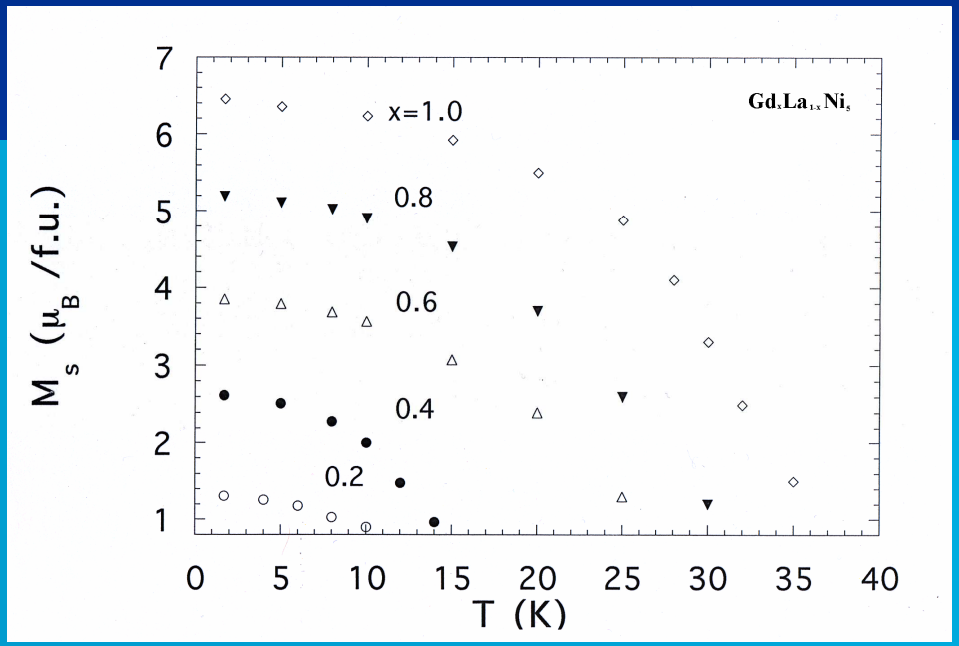

Fig.32

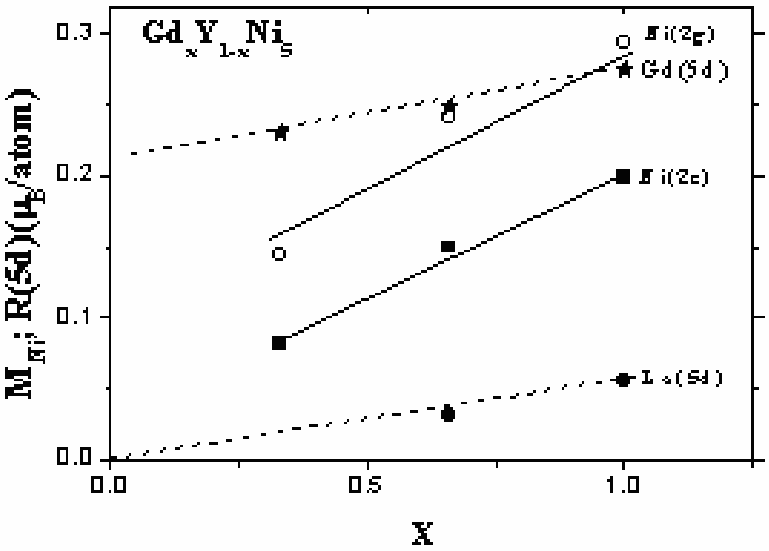

Fig.33

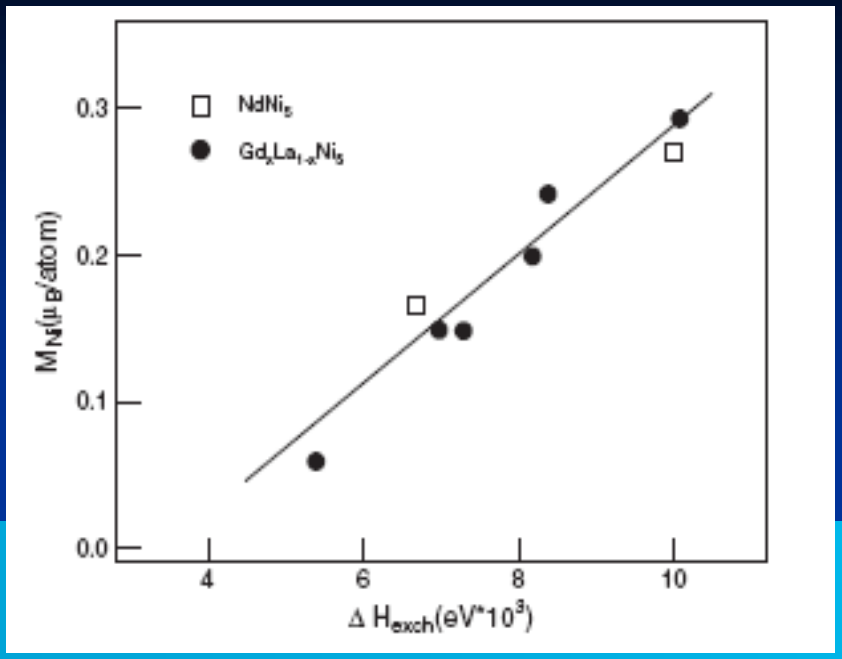

Fig.34

$H_c \cong 40$ T

$H_c \cong 30$ T

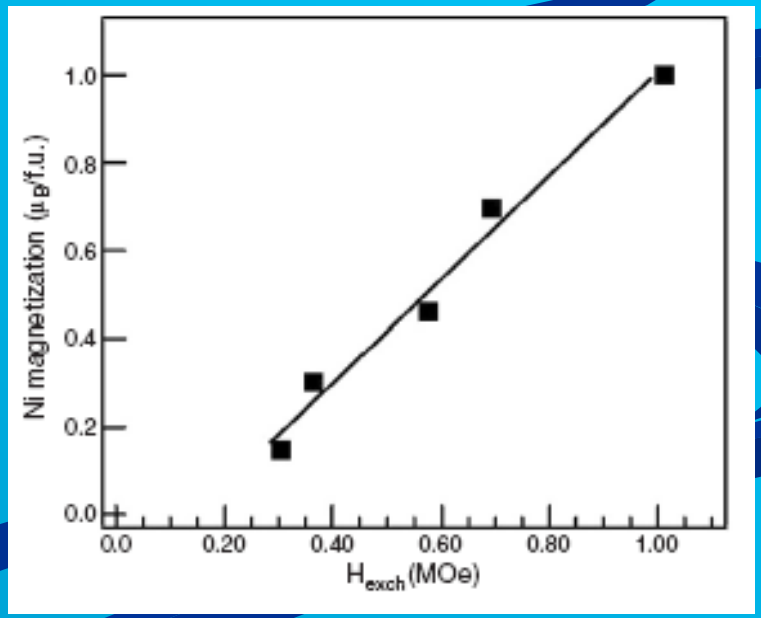

Fig.35

2.3 Exchange interactions

4f-5d-3d type (Campbell)

RM_2 compounds, R-heavy rare-earth

Fig.36

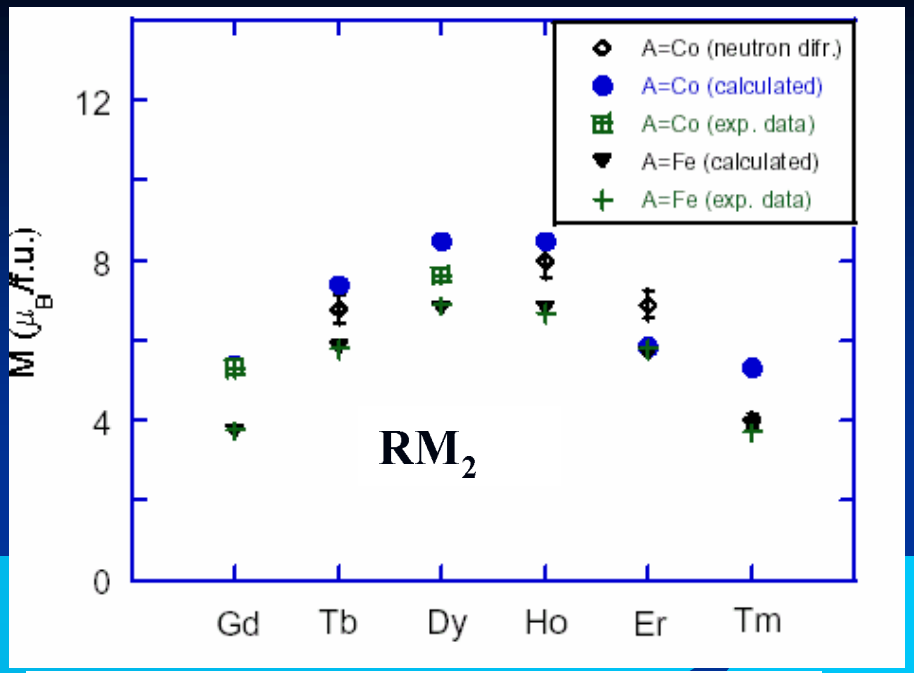

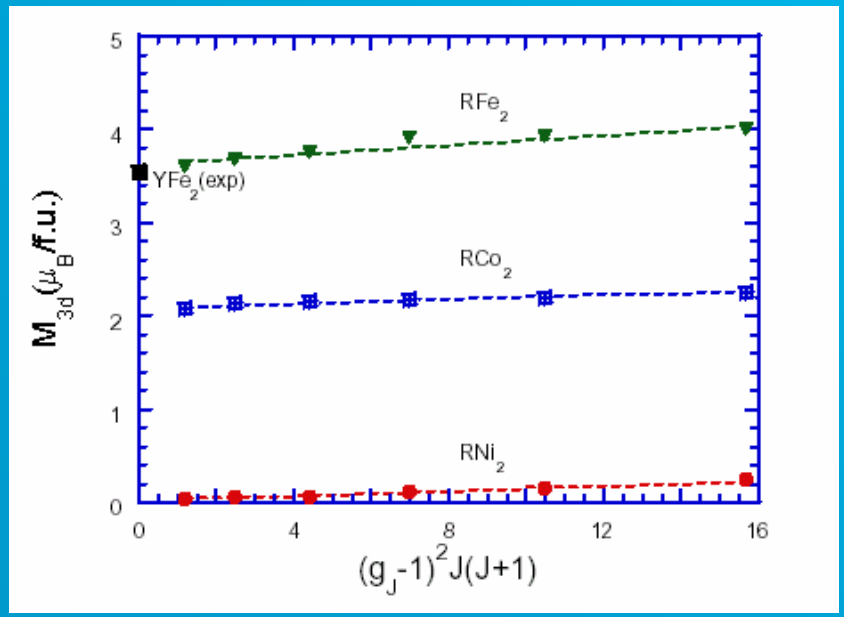

Fig.37

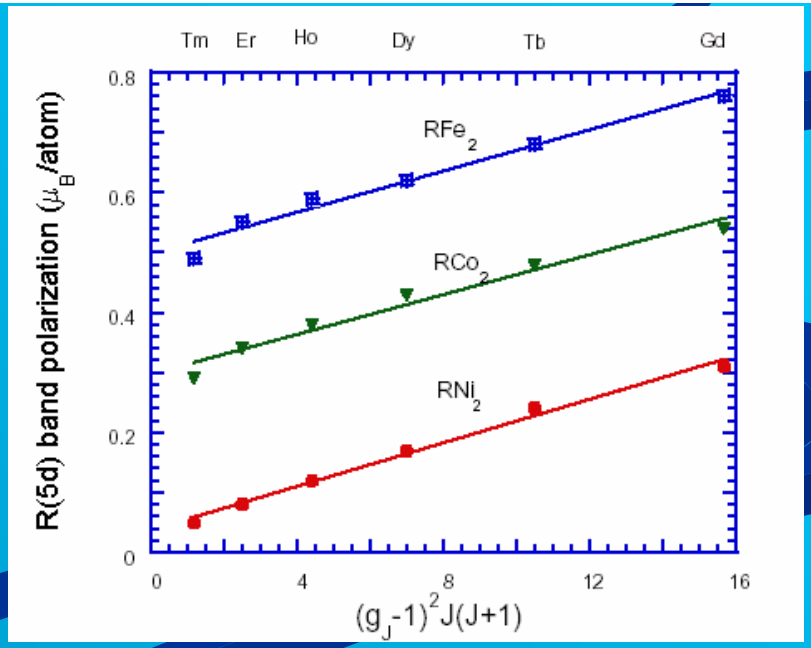

Fig.38

$M_{3d} \propto G$ $\quad G = (g_J-1)^2 J(J+1)$

$M_{5d} = M_{5d}(0) + \alpha G$

αG intra-atomic 4f-5d exchange

$M_{5d}(0)$ short range exchange interactions

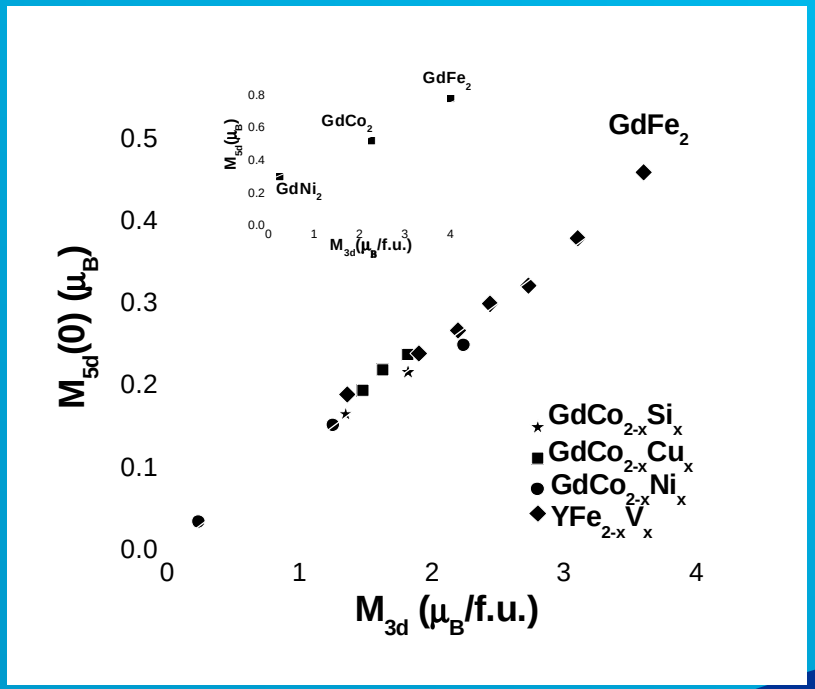

Fig.39

RM_5 M=Co, Ni

$M_{5d}=M_{5d}(0)+\alpha' G$ $\alpha'=1.4\cdot10^{-2}\mu_B$

$M_{5d}(0)=0.32$ Co

$=0.08$ Ni

$M_{3d}=M_{3d}(0)+\beta' G$ $\beta'=1\cdot10^{-2}\mu_B$ Co

$=1.6\cdot10^{-2}\mu_B$ Ni

$M_{5d}(0)/M_{3d}(0)=0.045$

RCo_4B, RM_5

$$H=\sum_{i=1}^{2} J_{3d_i-5d} S_{5d}(0) \sum_n S_{3d_i,n} + J_{5d-5d} S_{5d} \sum_{i=1}^{2} S_{5d_i}$$

$$\Downarrow$$

$$\Delta M_{5d}(0) \propto H_{exch} \propto \sum_i n_i M_{i_c}$$

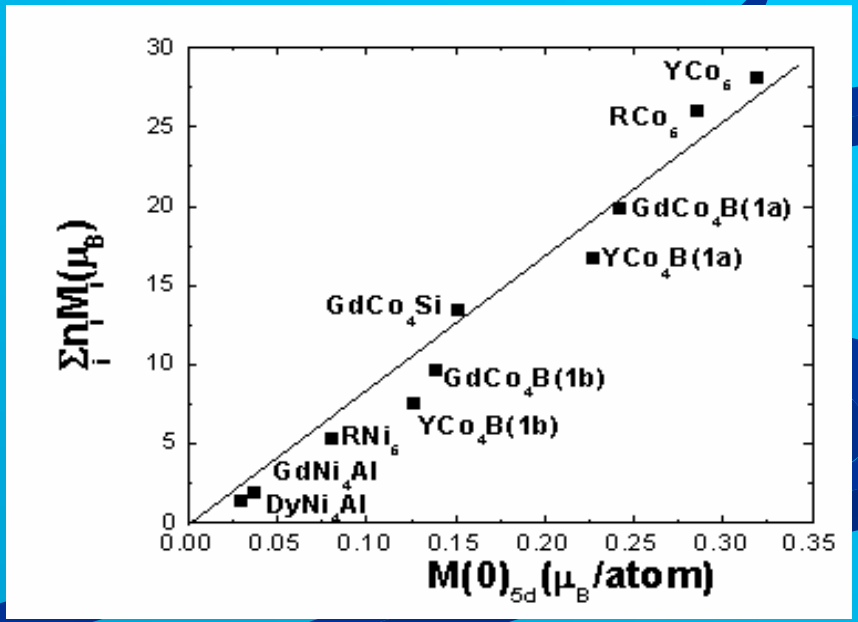

Fig.40

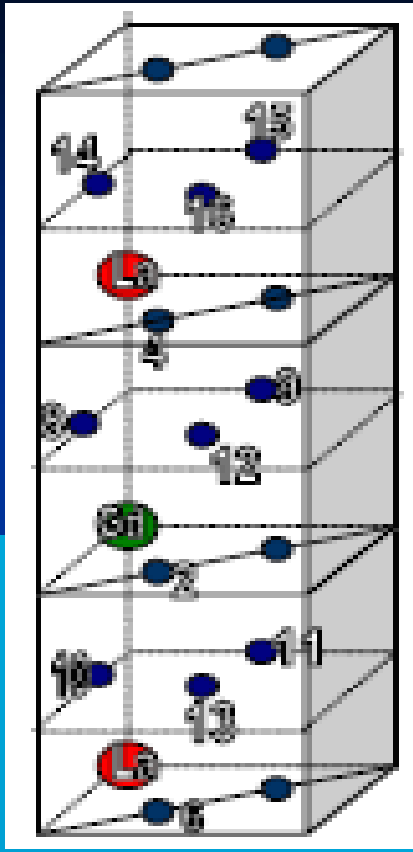

Fig.41

$$J_{ij} = \sum_{\{m\}} I^{i}_{mm'} \chi^{ij}_{mm'm''m'''} I^{j}_{m''m'''}$$

where the spin dependent potentials, I^i, are expressed in terms of the single particle potential $V_{mm'}$: $I^{i}_{mm'} = V^{i\uparrow}_{mm'} - V^{i\downarrow}_{mm'}$, while the effective inter-sublattice susceptibilities, χ^{ij}, were defined in terms of the LDA eigenfunctions as

$$\chi^{ij}_{mm'm''m'''} = \sum_{knn'} \frac{n_{nk\uparrow} - n_{n'k\downarrow}}{\varepsilon_{nk\uparrow} - \varepsilon_{n'k\downarrow}} \Psi^{ilm*}_{nk\uparrow} \Psi^{ilm''}_{nk\uparrow} \Psi^{ilm'}_{n'k\downarrow} \Psi^{jlm*}_{nk\downarrow} .$$

We denoted by n_i the orbital occupancy of d electrons, l the orbital quantum number and m the magnetic quantum number.

$GdNi_5$

$J_{3g\text{-}3g}(1) = 57$ K

$J_{3g\text{-}3g}(2) = 28$ K

$J_{2c\text{-}3g}(1) = 26$ K

$GdLa_2Ni_{15}$

$J_{3g\text{-}3g}$(La) (14-15) 37 K

(14-16) 18 K

(15-16) 11 K

$J_{2c\text{-}3g}$(La) (4-14) 23 K

(4-16) 19 K

(4-15) 7 K

$J_{3g\text{-}3g}$(Gd) (8-9) 40 K

(8-12) 23 K

(9-12) 17 K

$J_{2c\text{-}3g}$(Gd) (2-8) 24 K

(2-12) 21 K

(2-9) 9 K

Rhodes-Wohlfart curve

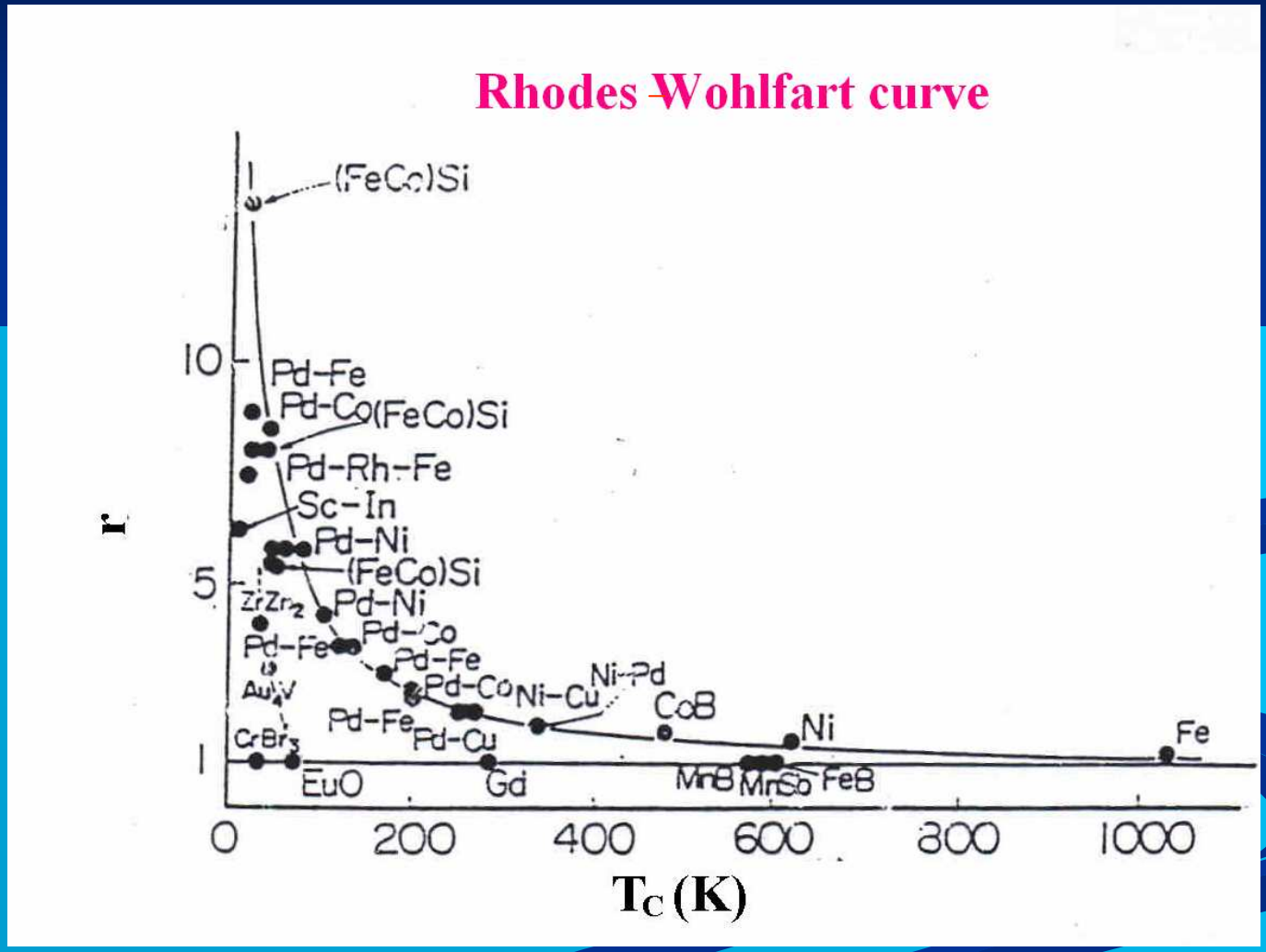

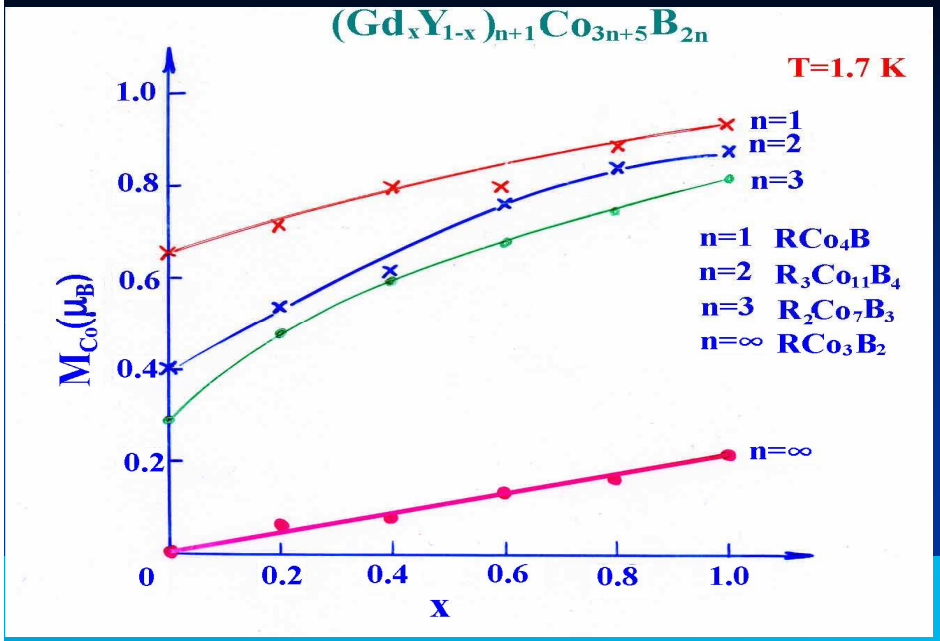

Fig.42

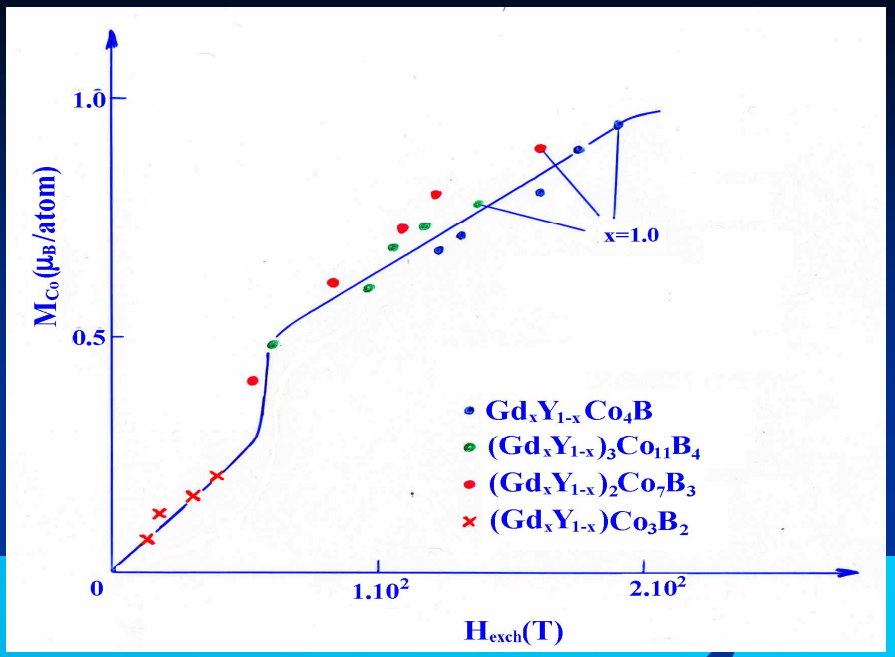

Fig.44

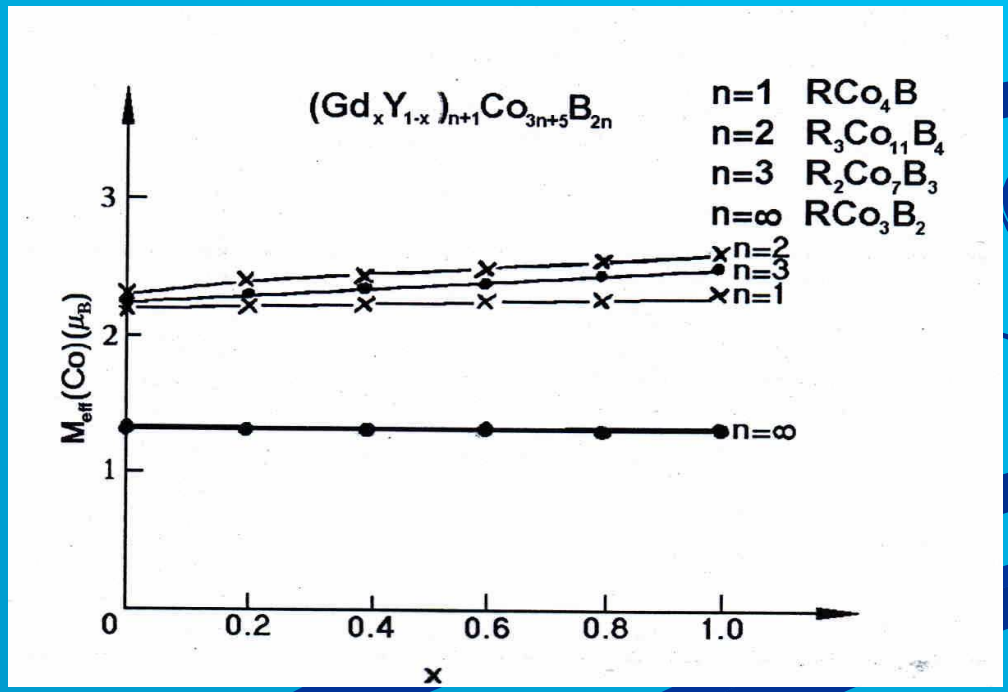

Fig.43

Both longitudinal and transverse components of the local spin fluctuations.

Relative contributions given by $r = S_p/S_o$ between the number of spins determined from effective moments $\mu_{eff} = g\sqrt{S_p(S_p+1)}$ and that obtained from saturation data $\mu_s = gS_o$

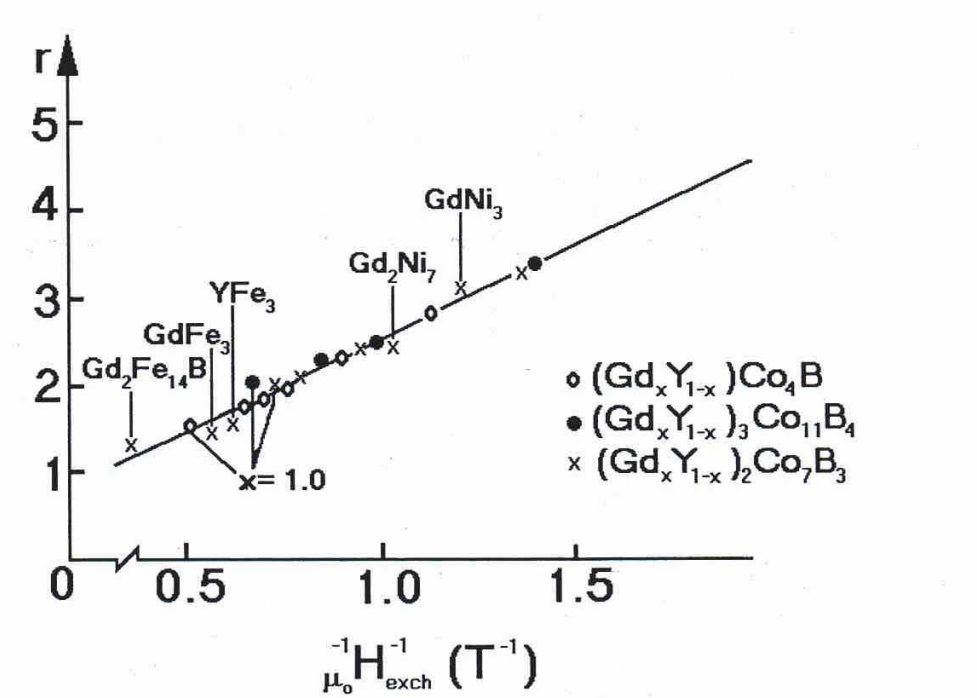

Mechanisms:

- increase of saturation Co and Ni moments as exchange fields increase
- gradual quenching of spin fluctuations by internal field, diminishing the effective moments

3. Technical Applications

3.1 Permanent Magnets:

- Cobalt based magnets

a) RCo_5, R_2Co_{17}- based magnets: light rare – earths

RCo_5 $T_C \cong 1000$ K

R_2Co_{17} $T_C \cong 1150$ K

R = Sm high uniaxial anisotropy

Expensive: natural abundance of Sm, Co

(BH)max $\cong 200$ kJ/m^3

$\cong 240$ kJ/m^3

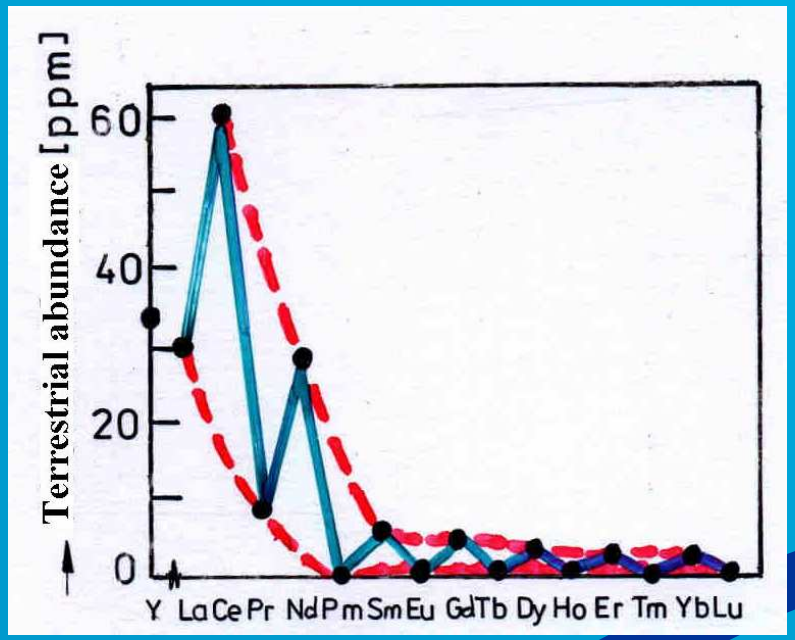

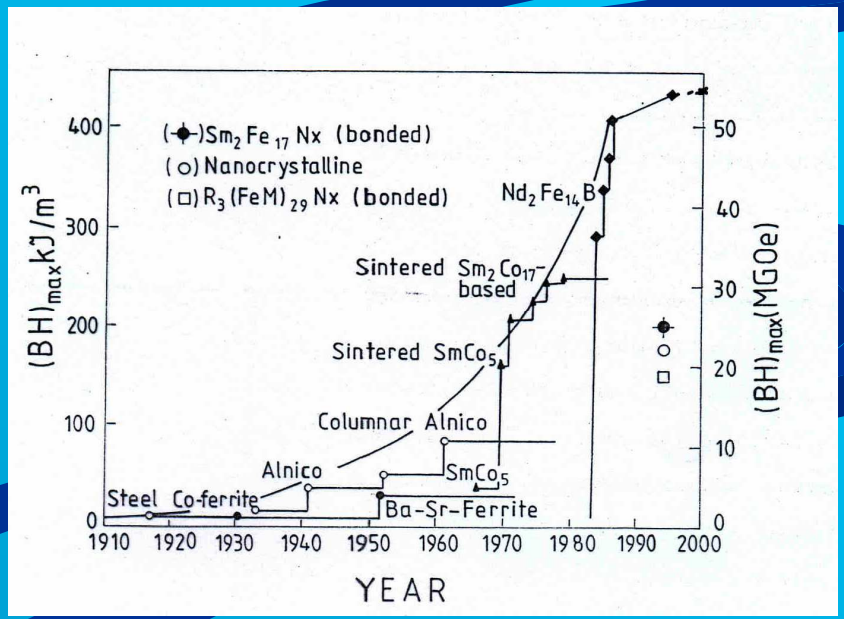

$SmCo_5$

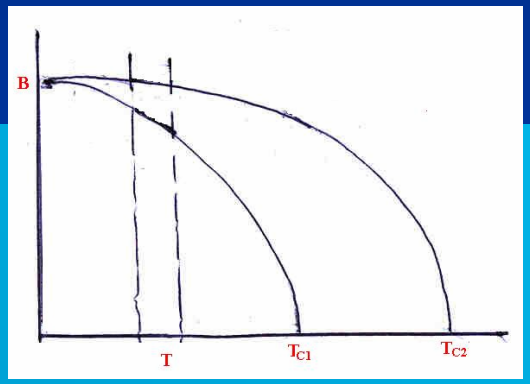

Fig.46

$Sm_2(Co,M)_{17}$

M=Fe,Zr,Cu

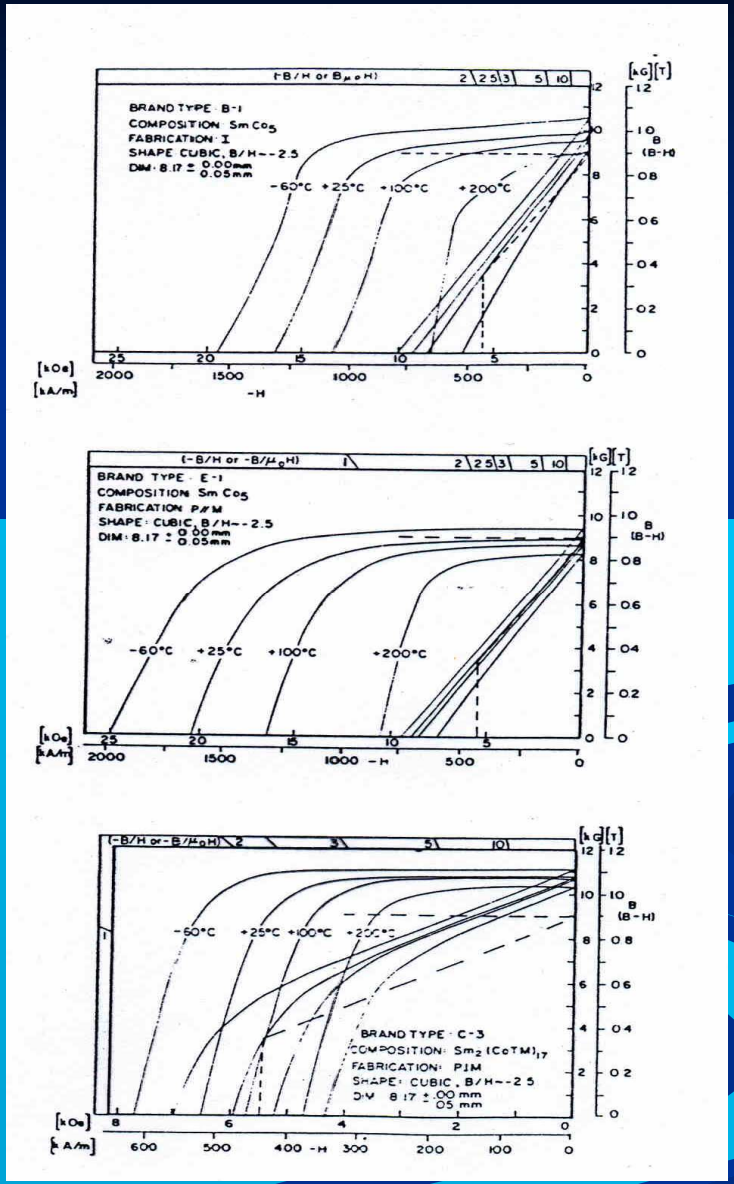

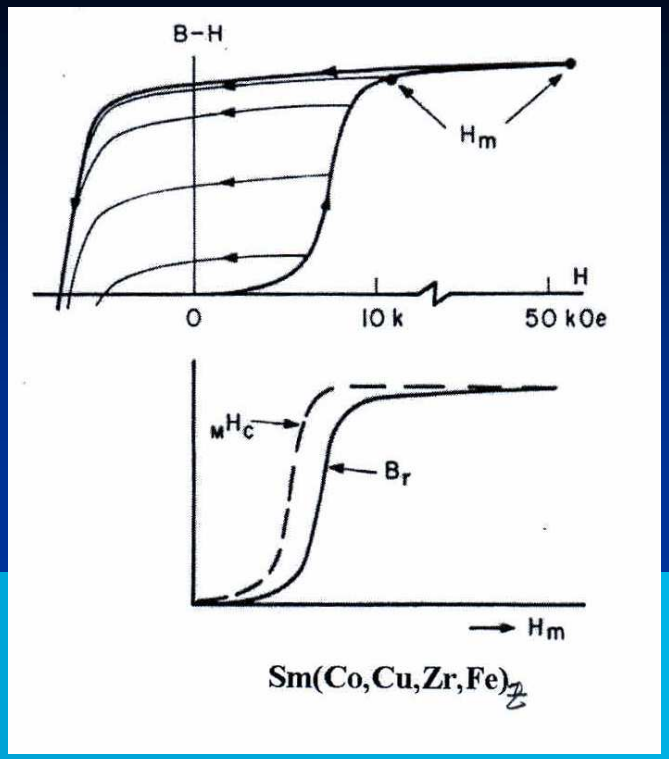

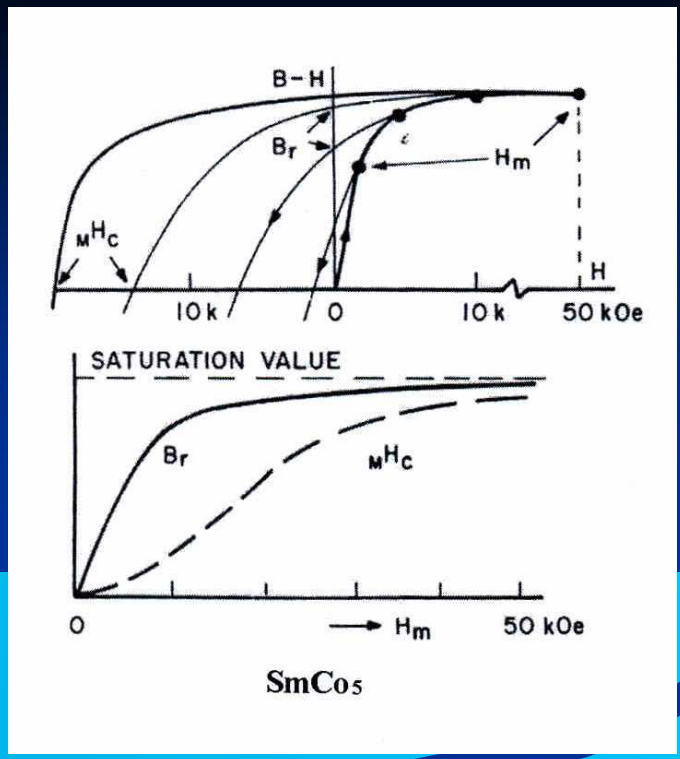

Pinning process

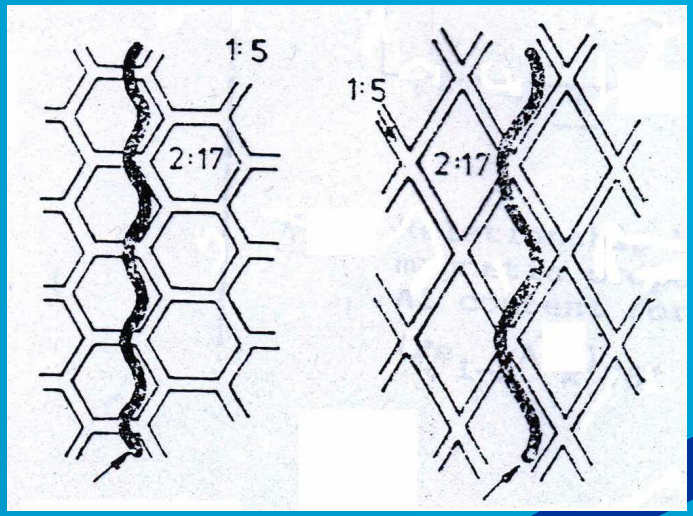

Nucleation process

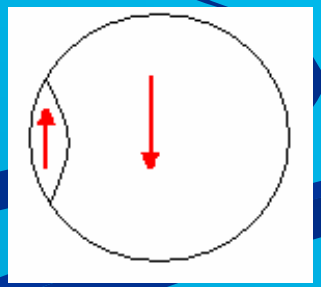

Fig.47

- iron based: Nd-Fe-B
  - low Curie points, $T_C \cong 580$ K
  - high energy product at RT

    $(BH)_{max} \cong 420$ kJ/m^3
  - high decrease of energy product with T

    T<100 ^oC
  - low cost

Fig.48

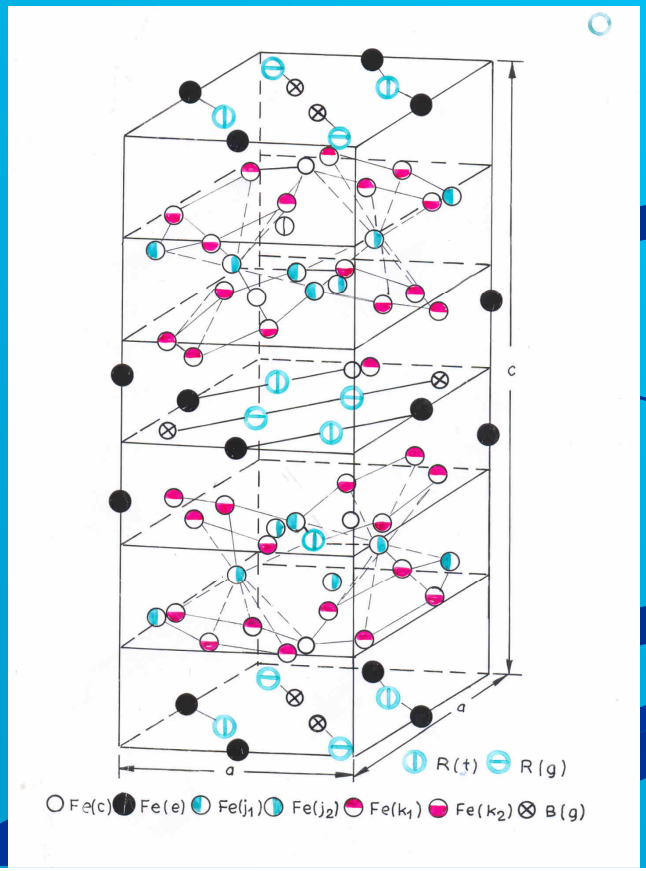

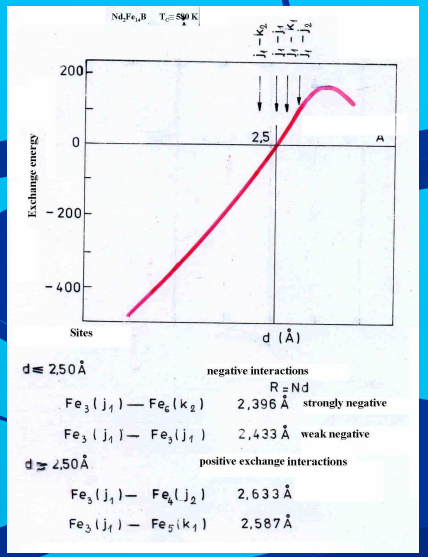

Nd-Fe-B sintered magnets

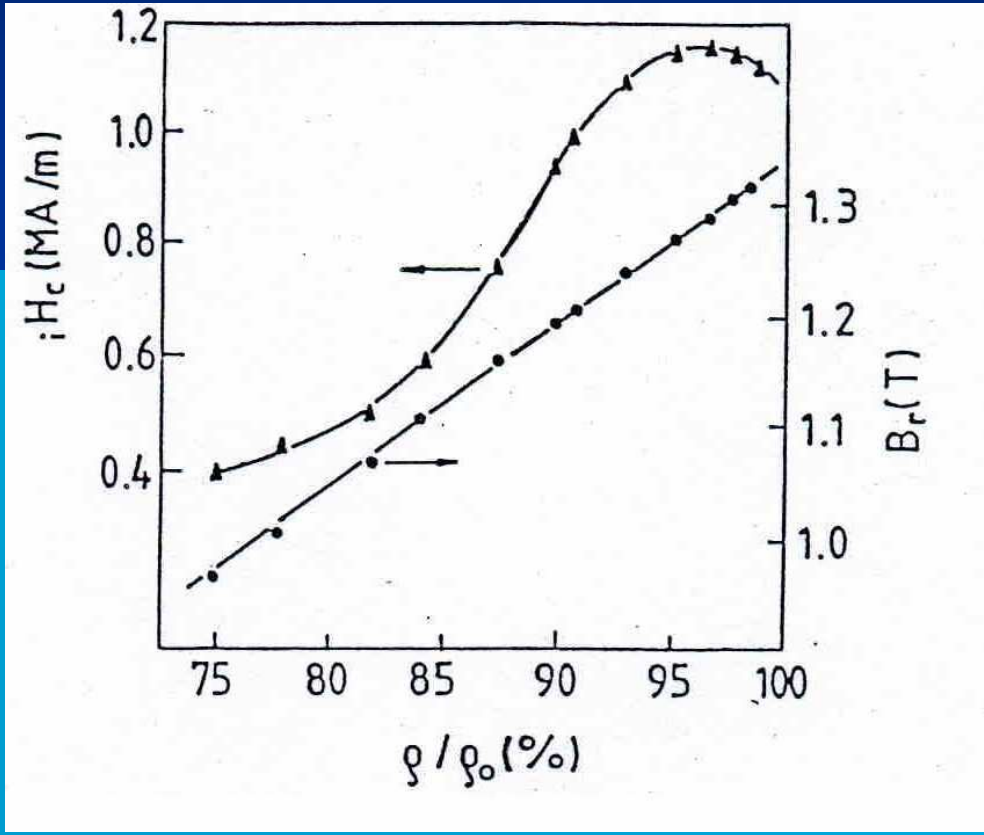

Fig.49

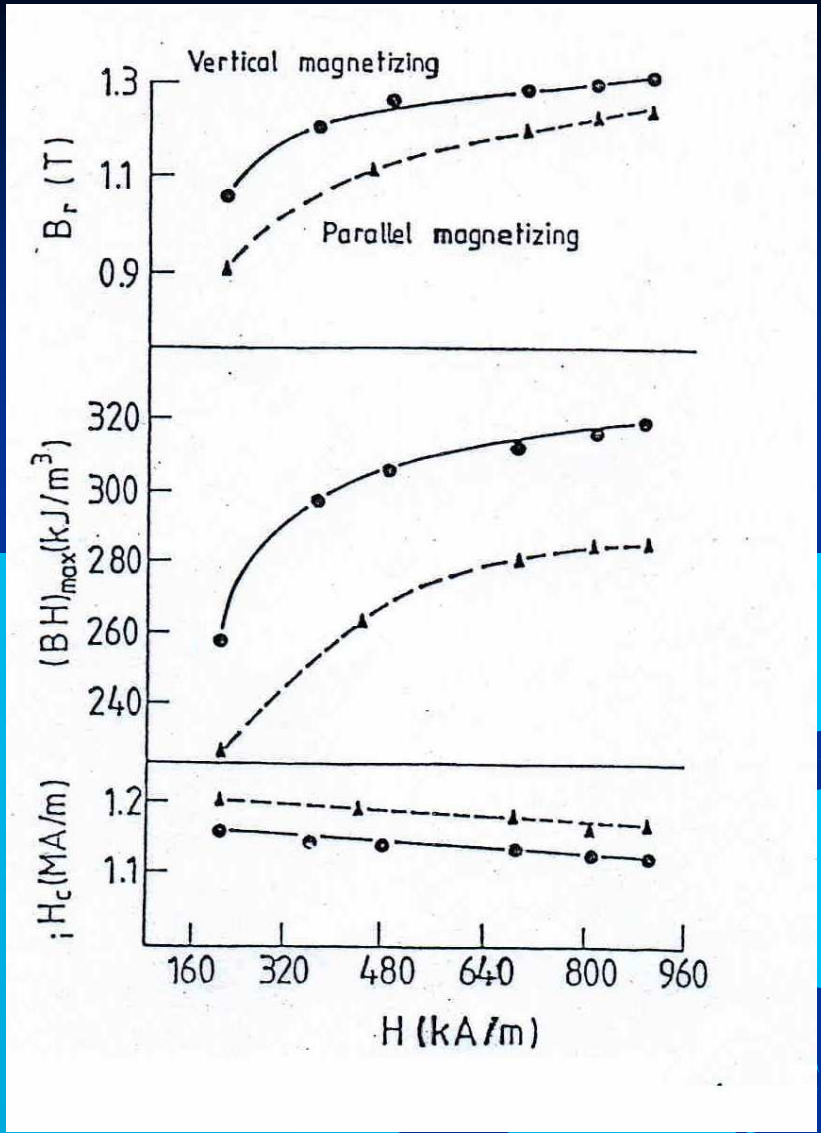

Fig.50

Nanocrystalline magnets

Isotropic microcrystalline Nd-Fe-B ribbons

$B_r \cong B_s/2$

Alloys with low Nd content

grain refinement into nanocyrstalline regime increase B_r

$B_r > B_s/2$

less expensive permanent magnets

- High boron content $Nd_{4.5}Fe_{77}B_{18.5}$:Ex

  $Nd_2Fe_{14}B + Fe_3B + \alpha$-Fe

- Low boron content $Nd_6Fe_{88}B_6$:Ex

  $Nd_2Fe_{14}B + \alpha$-Fe

Mean grain sizes

$Nd_2Fe_{14}B$ (< 30 nm) :d_n

Soft magnetic phase (< 15 nm) :d_n

Exchange coupling reduces the resistance to reversal magnetization but not lead to:

- collapse of H_C
- deteriorated (BH) loop

Condition: dimension of soft magnetic phase < exchange distance for the phase

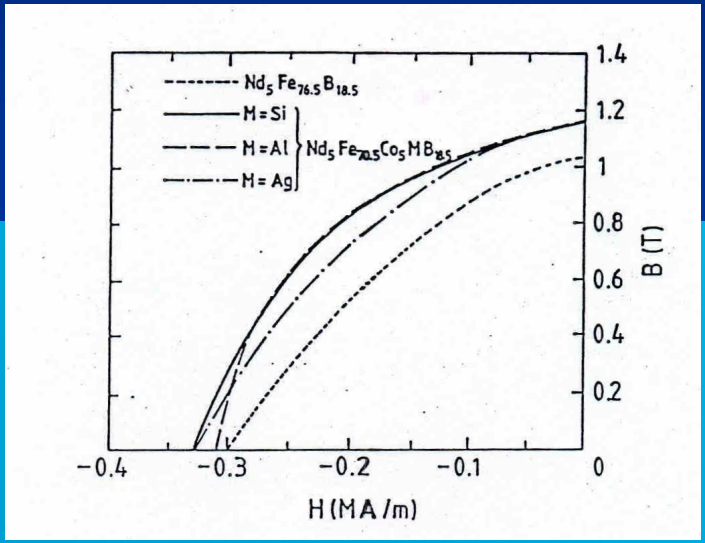
Nd5 Fe76.5 B18.5
M = Si
M = Al
M = Ag
Nd5 Fe70.5 Co5 M B18.5
1.4
1.2
1
0.8
0.6
0.4
0.2
0
B (T)
−0.4
−0.3
−0.2
−0.1
H (MA/m)

Fig.51

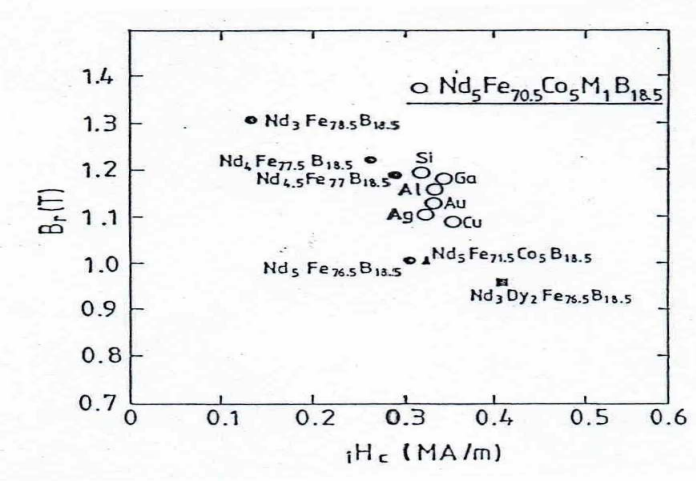
o Nd5 Fe70.5 Co5 M1 B18.5
Nd3 Fe78.5 B18.5
Nd4 Fe77.5 B18.5
Nd4.5 Fe77 B18.5
Si
Al
Ga
Au
Ag
Cu
Nd5 Fe71.5 Co5 B18.5
Nd5 Fe76.5 B18.5
Nd3 Dy2 Fe76.5 B18.5
1.4
1.3
1.2
1.1
1.0
0.9
0.8
0.7
Br (T)
0
0.1
0.2
0.3
0.4
0.5
0.6
iHc (MA/m)

Fig.52

3.2 Magnetostrictive materials

Rare-Earths (R)

- interesting properties for technical applications
- low Curie temperatures $T_C \leq 300$ K

$\lambda^{\varepsilon,2}$ = $8.8 \cdot 10^{-3}$ Tb

4.2 K $8.8 \cdot 10^{-3}$ Dy

$2.5 \cdot 10^{-3}$ Ho

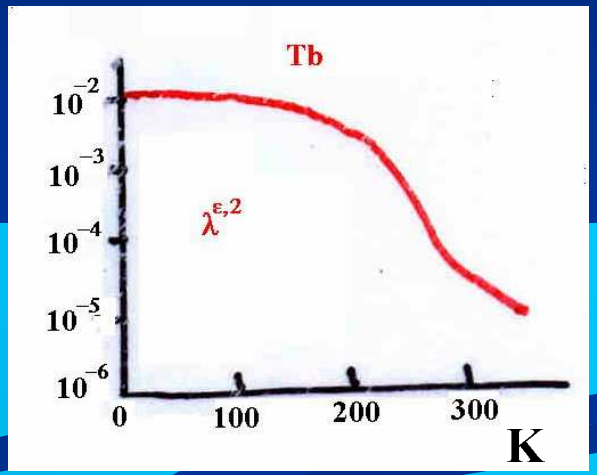

- cannot be used for devices working at RT

Rare-Earth-Transition Metal Compounds: RM_x M= Fe,Co

On the support of exchange interactions the R useful properties translated at higher T

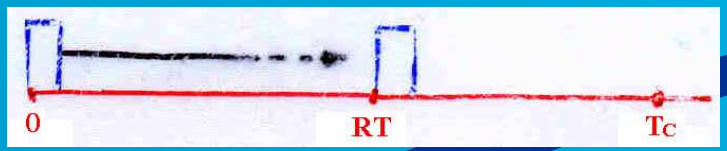

R-Fe compounds

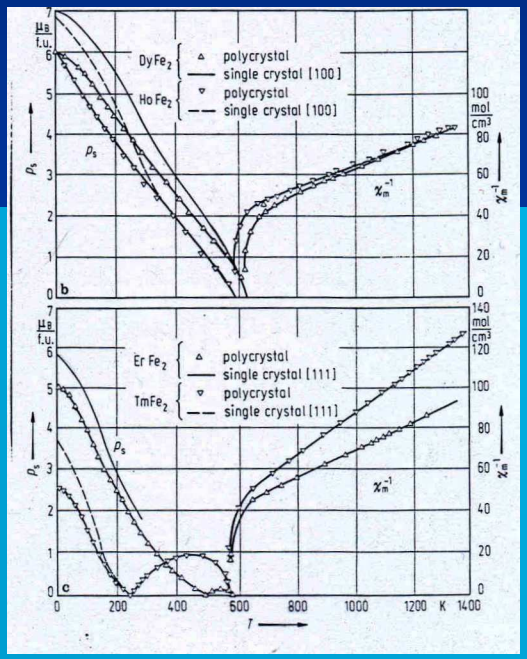

Fig.53

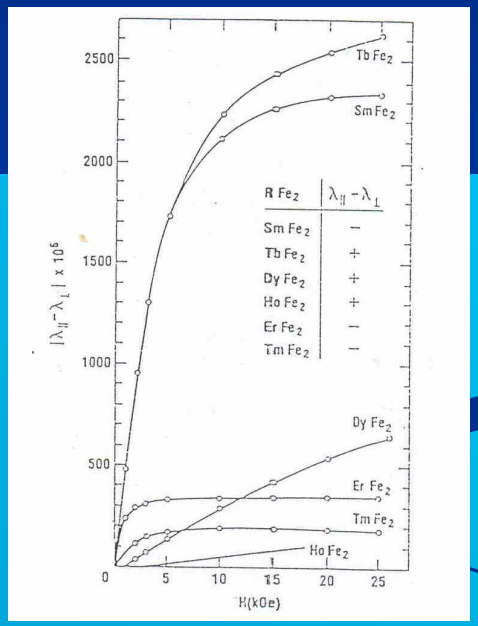

Fig.54

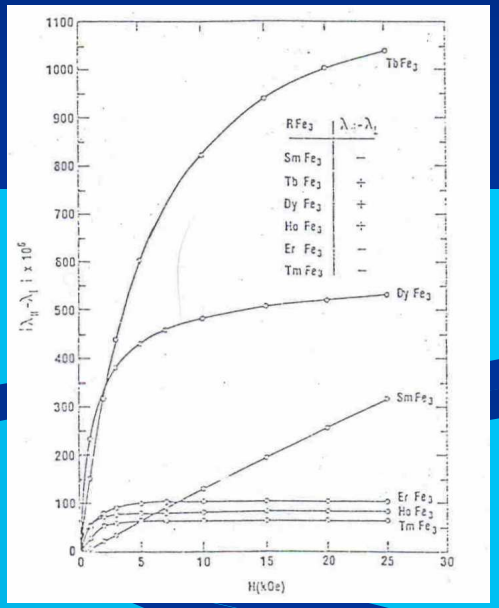

Fig.55

$TbFe_2$ high anisotropy: high magnetostriction

Minimizing magnetic anisotropy but maintaining a large magnetostriction

- opposite sign of anisotropy (anisotropy compensating system)

$Tb_{0.27}Dy_{0.73}Fe_2$

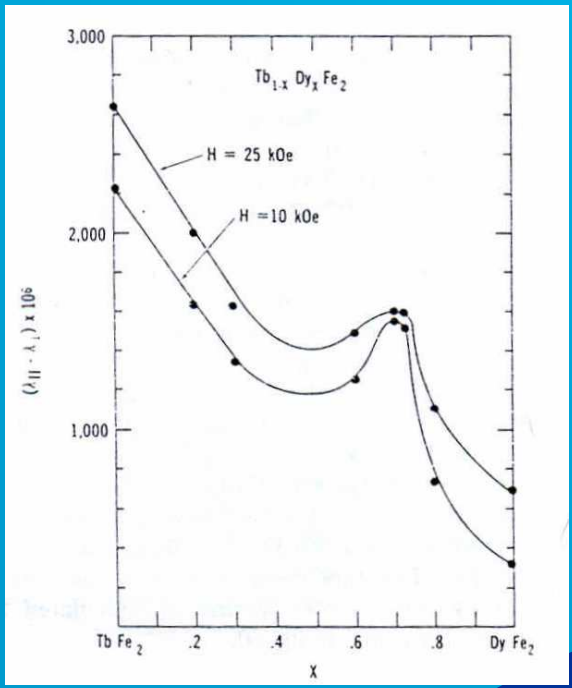

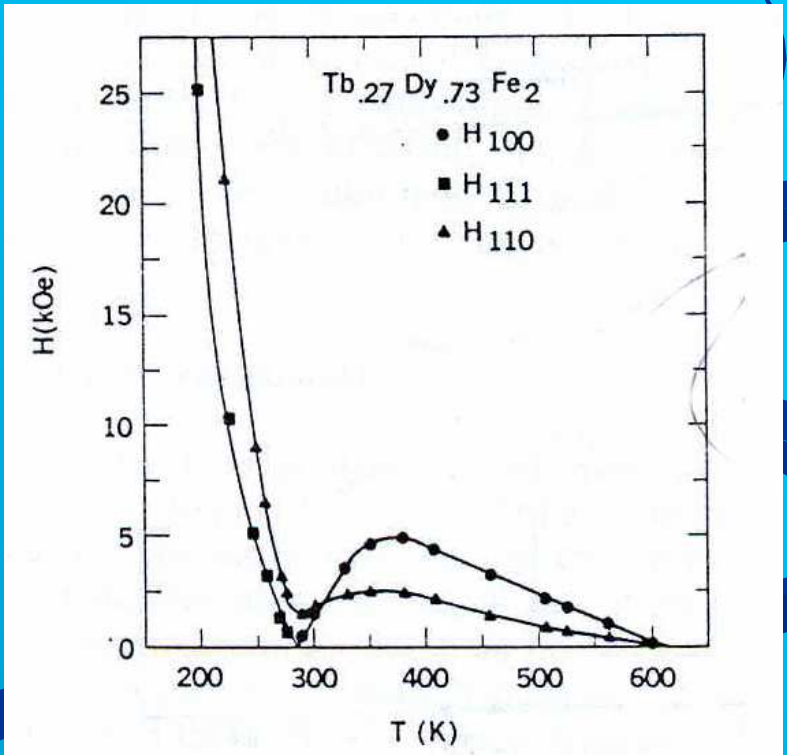

3.3. Magnetocaloric effects

The isothermal magnetic entropy changes, $\Delta S_M(T,\Delta H)$

$$\Delta S_M(T,\Delta H) = \int_0^{\Delta H} \left(\frac{\partial M}{\partial T}\right)_H dH$$

Discrete fields and temperature intervals

$$\Delta S_M = \sum \frac{1}{T_{i+1}-T_i}(M_{i+1} - M_i)_H \Delta H_i$$

From magnetic measurements ΔS_M were evaluated

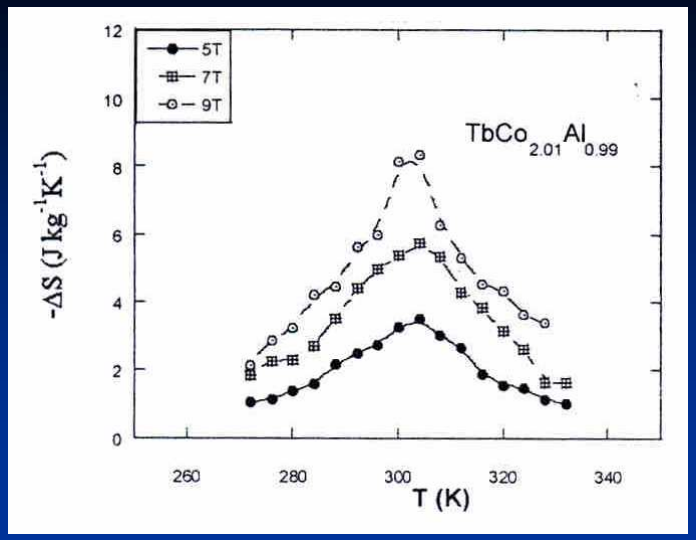

Fig.56

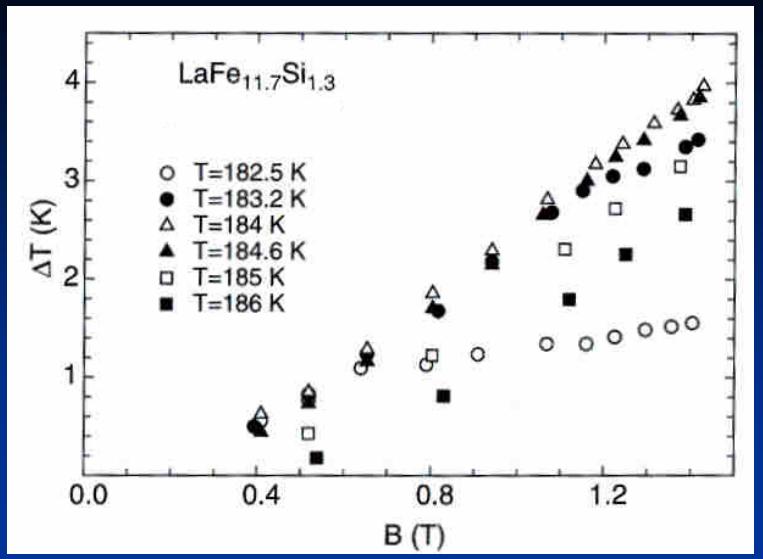

Fig.57

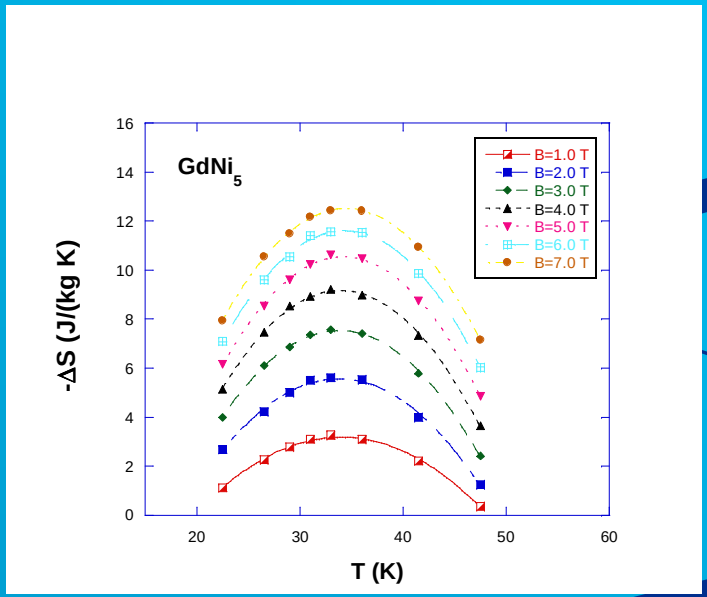

Fig.58

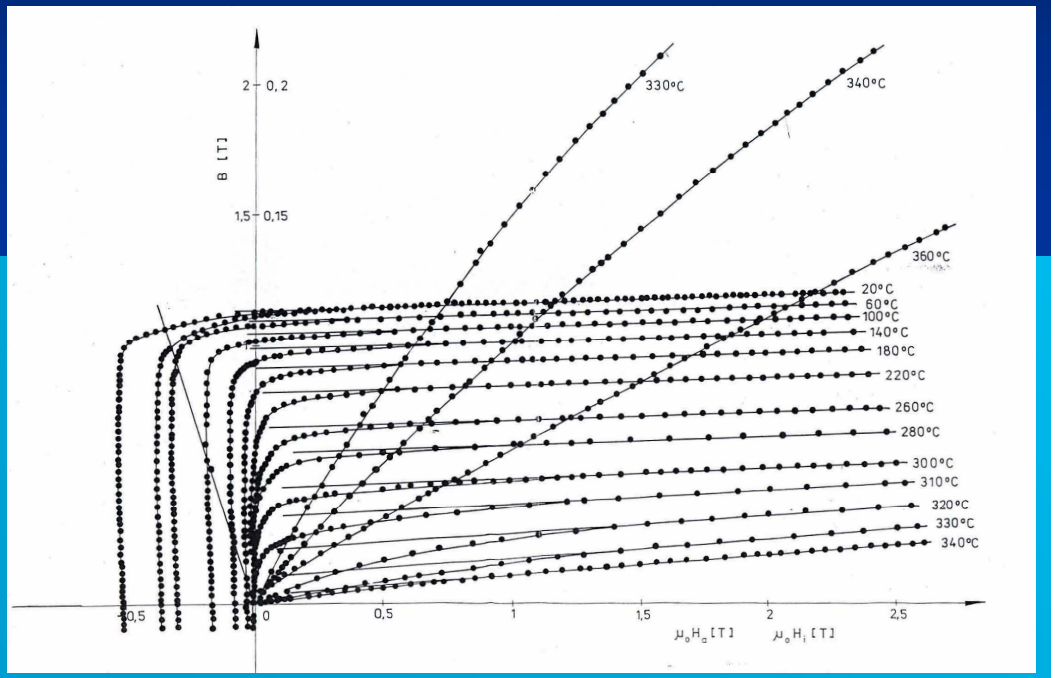
B [T]
2
0,2
1,5
0,15
330°C
340°C
360°C
20°C
60°C
100°C
140°C
180°C
220°C
260°C
280°C
300°C
310°C
320°C
330°C
340°C
-0,5
0
0,5
1
1,5
2
2,5
μ0Ha [T]
μ0Hi [T]

Fig.60

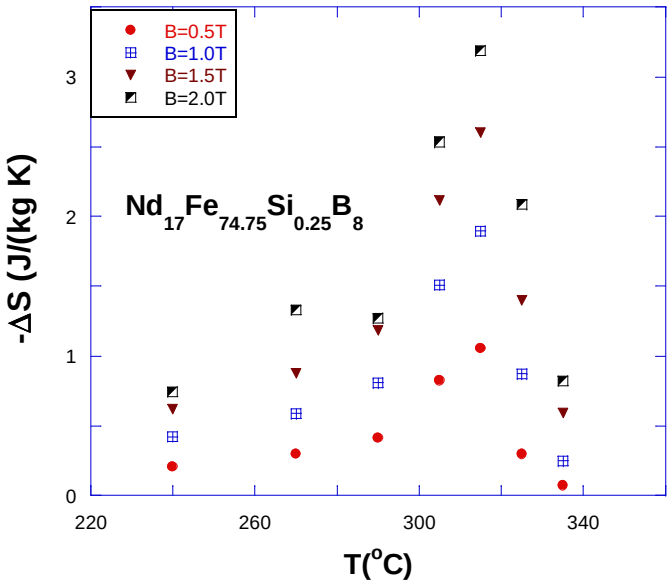
B=0.5T
B=1.0T
B=1.5T
B=2.0T
Nd17Fe74.75Si0.25B8
-ΔS (J/(kg K)
0
1
2
3
220
260
300
340
T(°C)

Fig.61

3.4 Hydrogen in Metals

$LaNi_5$ shows an absorption plateau pressure of few bars at RT. There is a complete revesibility between formation and decomposition with a hysteresis between the corresponding equilibrium pressure. An α–phase s.s. precedes β-$LaNi_5H_6$ hydride. The system requires an activation stage which involves decrepitation into small particles.

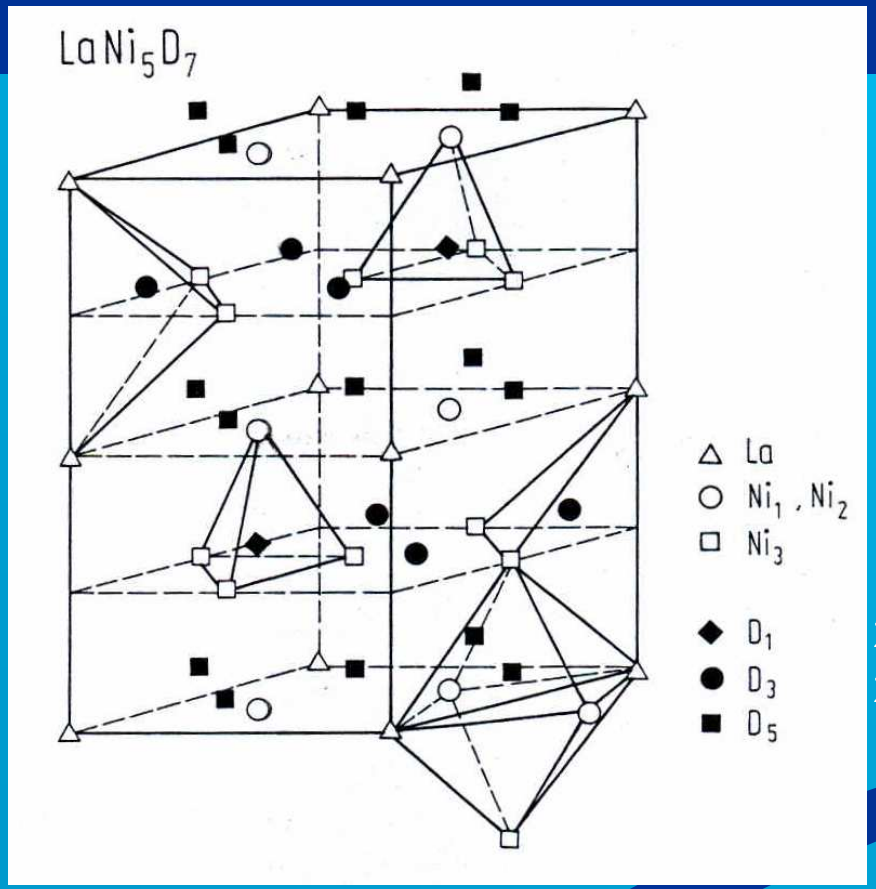

Fig.62

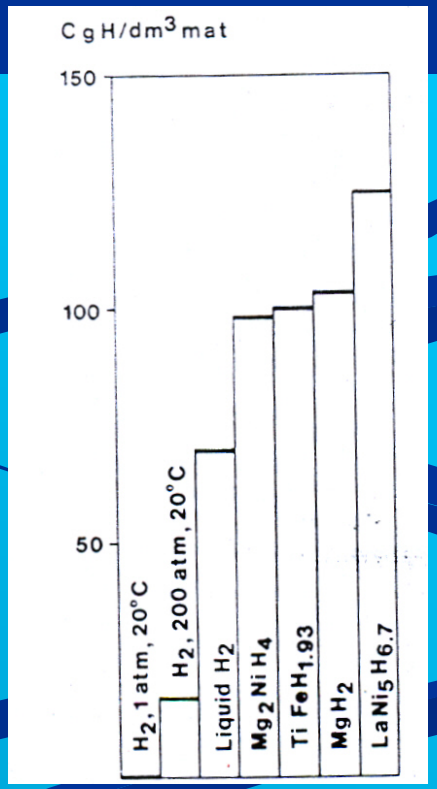

Fig.63

Thank you very much for your attentions.